© 2015. Published by The Company of Biologists Ltd | Journal of Cell Science (2015) 128, 2766-2780 doi:10.1242/jcs.167775

RESEARCH ARTICLE

Phosphorylation of PACSIN2 by protein kinase C triggers the removal of caveolae from the plasma membrane

Yosuke Senju[1,*], Eva Rosenbaum[2], Claudio Shah[2], Sayaka Hamada-Nakahara[1], Yuzuru Itoh[1], Kimiko Yamamoto[3], Kyoko Hanawa-Suetsugu[1,4], Oliver Daumke[2] and Shiro Suetsugu[1,4,‡]

ABSTRACT

PACSIN2, a membrane-sculpting BAR domain protein, localizes to caveolae. Here, we found that protein kinase C (PKC) phosphorylates PACSIN2 at serine 313, thereby decreasing its membrane binding and tubulation capacities. Concomitantly, phosphorylation decreased the time span for which caveolae could be tracked at the plasma membrane (the 'tracking duration'). Analyses of the phospho-mimetic S313E mutant suggested that PACSIN2 phosphorylation was sufficient to reduce caveolar-tracking durations. Both hypotonic treatment and isotonic drug-induced PKC activation increased PACSIN2 phosphorylation at serine 313 and shortened caveolar-tracking durations. Caveolar-tracking durations were also reduced upon the expression of other membrane-binding-deficient PACSIN2 mutants or upon RNA interference (RNAi)-mediated PACSIN2 depletion, pointing to a role for PACSIN2 levels in modulating the lifetime of caveolae. Interestingly, the decrease in membrane-bound PACSIN2 was inversely correlated with the recruitment and activity of dynamin 2, a GTPase that mediates membrane scission. Furthermore, expression of EHD2, which stabilizes caveolae and binds to PACSIN2, restored the tracking durations of cells with reduced PACSIN2 levels. These findings suggest that the PACSIN2 phosphorylation decreases its membrane-binding activity, thereby decreasing its stabilizing effect on caveolae and triggering dynamin-mediated removal of caveolae.

KEY WORDS: Caveolae, BAR domain, Phosphorylation, Protein kinase C, Mechanical stress

INTRODUCTION

Proteins containing a membrane-sculpting Bin-Amphiphysin-Rvs (BAR) domain are evolutionarily conserved, and members of this family are found at various intracellular membrane structures, including clathrin-coated pits, compartments of the endocytic pathways, and membrane protrusions, such as filopodia and lamellipodia (Safari and Suetsugu, 2012; Suetsugu et al., 2014). BAR domain proteins form crescent-shaped homodimers and sense or generate membrane curvature through positively charged surfaces (Frost et al., 2008, 2009; Itoh and De Camilli, 2006; Peter et al., 2004; Suetsugu et al., 2010), thereby performing crucial roles in membrane remodeling. During these processes, BAR domain proteins polymerize into helical coats through lateral and tip-to-tip interactions to deform the membrane into a tubular shape (Frost et al., 2008; Shimada et al., 2007). However, it is often unclear how assembly and disassembly of BAR domain proteins is regulated.

The F-BAR-domain-containing proteins form a subfamily of the BAR domain family. The three paralogs of the F-BAR-domain-containing PACSIN family (for Protein kinase C and casein kinase substrate in neuron protein, also called syndapin) display different expression patterns. PACSIN1 is restricted to neural tissues and is implicated in synaptic vesicle recycling (Kessels and Qualmann, 2004; Qualmann et al., 1999), PACSIN2 is ubiquitously expressed, and PACSIN3 is mainly found in skeletal muscles (Modregger et al., 2000). Previous studies have reported that PACSIN2 regulates the morphogenesis and endocytosis of caveolae (Hansen et al., 2011; Koch et al., 2012; Senju et al., 2011). PACSIN2 contains an N-terminal F-BAR domain that sculpts membranes into tubules through a positively charged concave surface and hydrophobic insertions into the membrane (Peter et al., 2004; Shimada et al., 2010). Intramolecular interactions between the F-BAR and SH3 domains of PACSINs have been proposed to have an auto-inhibitory function (Rao et al., 2010) to suppress membrane binding and tubulation (Shimada et al., 2010; Takeda et al., 2013; Wang et al., 2009). The C-terminal SH3 domain of PACSIN2 associates with the proline-rich domain (PRD) of dynamin 2, providing a possible link between caveolae and dynamin-2-mediated membrane scission (Daumke et al., 2014; Senju et al., 2011; Suetsugu and Gautreau, 2012). Furthermore, the auto-inhibited conformation of PACSINs is thought to be opened by this interaction, thereby increasing the membrane-binding affinity and membrane-tubulating activity of PACSIN2 (Rao et al., 2010; Senju et al., 2011; Wang et al., 2009). The SH3 domain of PACSIN also interacts with the Arp2/3 activator N-WASP, which has been suggested to promote actin polymerization at the plasma membrane (Kessels and Qualmann, 2002). However, it was later suggested that N-WASP and the Arp2/3 complex do not connect caveolae to actin filaments (Echarri et al., 2012). PACSIN2 also binds the dynamin-related EHD2 ATPase, through an asparagine-proline-phenylalanine (NPF) sequence in the linker between the F-BAR and SH3 domains (Braun et al., 2005). EHD2, in turn, has been shown to interact with the caveolar coat protein cavin 1 (also known as PTRF) (Moren et al., 2012). Furthermore, EHD2 is thought to localize to the necks of caveolae, thereby stabilizing caveolae at the plasma membrane (Ludwig et al., 2013; Moren et al., 2012; Stoeber et al., 2012).

Phosphorylation of *Drosophila* PACSIN (Syndapin) in the linker region has been reported to reduce its membrane binding, which might have functions related to the control of cytokinesis (Takeda et al., 2013). PACSIN1 phosphorylation has also been reported to

[1]Laboratory of Membrane and Cytoskeleton Dynamics, Institute of Molecular and Cellular Biosciences, University of Tokyo, 1-1-1 Yayoi, Bunkyo-ku, Tokyo 113-0032, Japan. [2]Crystallography, Max Delbrück Center for Molecular Medicine, Berlin 13125, Germany. [3]Laboratory of System Physiology, Department of Biomedical Engineering, Graduate School of Medicine, University of Tokyo, Tokyo 113-0033, Japan. [4]Laboratory of Molecular Medicine and Cell Biology, Graduate School of Biosciences, Nara Institute of Science and Technology, Ikoma 630-0192, Japan. *Present address: Institute of Biotechnology, University of Helsinki, Helsinki 00014, Finland.

‡Author for correspondence (suetsugu@bs.naist.jp)

Received 17 December 2014; Accepted 12 June 2015

Journal of Cell Science

Journal of Cell Science (2015) 128, 2766-2780 doi:10.1242/jcs.167775

weaken membrane association, resulting in a substantial change in neuronal morphology (Quan et al., 2012). Furthermore, phosphorylation in the linker regions of mammalian PACSIN1 and PACSIN2 has been shown to regulate the interactions with PICK1, a BAR-domain-containing adaptor protein (Anggono et al., 2013). However, the effect of this phosphorylation on membrane binding has not been examined, and the kinases responsible for phosphorylation not investigated. Furthermore, despite its original discovery as a protein kinase C (PKC) substrate and the localization of PKC at caveolae (Mineo et al., 1998; Oka et al., 1997; Sharma et al., 2004; Smart et al., 1994, 1995), the phosphorylation of PACSINs by PKC has not been studied in detail.

In this study, we identified PKC as the kinase that phosphorylates a specific site in the linker region of PACSIN2. Phosphorylation could be induced by mechanical stimuli, such as hypotonic stress and shear stress. Furthermore, we found that the phosphorylation of PACSIN2 decreased its membrane binding and tubulation activities. We also show that PACSIN2 phosphorylation decreased the time span for which caveolae could be observed at the plasma membrane as assessed by total internal reflection fluorescence (TIRF) microscopy. Interestingly, release of PACSIN2 from the plasma membrane was correlated with an increase of dynamin 2 levels at the membrane, and dynamin inhibition restored the membrane localization of PACSIN2. These data suggest that there is a mechanistic link between PKC activity and caveolar dynamics.

RESULTS

PACSIN2 is phosphorylated by PKC upon hypotonic treatment

Previous studies have indicated that PACSIN2 localizes to caveolae (Hansen et al., 2011; Koch et al., 2012; Ludwig et al., 2013; Senju et al., 2011). We hypothesized that PACSIN2 recruitment to caveolae was regulated by phosphorylation. Using sequence analysis, we identified phosphorylation consensus sites in PACSIN2 for several kinases that become activated upon cellular stimuli, including protein kinase B (PKB, also known as AKT1) and PKC, glycogen synthase kinase-3 (GSK-3) and IκB kinase (IKK) β (Fig. 1A). The conserved serine residues in these sites were replaced with acidic amino acids, to mimic phosphorylation (Maciejewski et al., 1995; Xue et al., 2011). These mutants were then expressed as GFP fusion proteins in HeLa cells. Over-expressed PACSIN2 localizes to tubular membranous structures (Senju et al., 2011). Two phospho-mimetic mutants, S313E and S373D, showed reduced membrane recruitment and/or tubule formation (Fig. 1B,C). S313 and S373 are located in the linker between the F-BAR and SH3 domains, and are predicted phosphorylation sites for PKCα and IKKβ. *In vitro* kinase assays confirmed that S313 and S373 were the major phosphorylation sites for PKCα and IKKβ, respectively (Fig. 1D). The two identified serine residues in PACSIN2 appeared to be phosphorylated independently, because both the S313E and S373D mutants of PACSIN2 were phosphorylated as efficiently as wild-type (WT) PACSIN2 by IKKβ and PKCα, respectively (Fig. 1D). The phosphorylation of both sites were independently confirmed by western blotting, using antibodies specific for each phosphorylated site (Fig. 1E,F).

To further clarify the specificity of PKC to PACSIN2, we examined the phosphorylation of PACSIN2 paralogs. PACSIN1 and PACSIN3 were both inefficient targets of PKCα, consistent with the missing consensus phosphorylation site (Fig. 1G). We also examined the phosphorylation of dynamin 2, because the PRD of the brain-specific dynamin 1 is reportedly phosphorylated by PKCα (Powell et al., 2000; Robinson et al., 1993). However, the PRD of the ubiquitous dynamin 2 (amino acids 741–870) was not phosphorylated by PKCα in our assays (Fig. 1G).

S313 of PACSIN2 is phosphorylated upon hypotonic treatment, cell detachment and shear stress

Caveolae are thought to respond to hypotonic stress (Sinha et al., 2011), and PKC is activated under these conditions (Chou et al., 1998; Davenport et al., 1995; Hermoso et al., 2004; Liu et al., 2003). Using our antibodies targeting phosphorylated S313 or S373, we examined the phosphorylation status of PACSIN2 upon hypotonic stimuli. S313 phosphorylation in HeLa cells was readily and significantly increased after 1 min of hypotonic treatment, and then gradually decreased (Fig. 2A). Phosphorylation was dependent on PKC, because treatment of cells with the PKC-inhibitor bisindolylmaleimide (BIM) prevented phosphorylation. Furthermore, S313 phosphorylation was significantly increased when PKC was artificially activated by drugs, such as phorbol-12-myristate-13-acetate (PMA), δ-amyloid precursor protein modulator (APP) or indolactam (Fig. 2B). In contrast, we did not find clear evidence for phosphorylation at S373 under these conditions (Fig. 2A,B). Therefore, in subsequent studies, we focused on the role of S313 phosphorylation.

To determine the physiological relevance of PACSIN2 phosphorylation, we examined phosphorylation upon cell detachment and shear stress application. Uptake of caveolae has previously been shown to be associated with cell detachment from the substratum (Del Pozo and Schwartz, 2007). We observed significant phosphorylation of endogenous PACSIN2 upon detachment of cells from their substratum by trypsin treatment (Fig. 2C). Phosphorylation was suppressed by treatment with BIM. Shear stress is also known to increase membrane tension in cells (Chachisvilis et al., 2006; Obi et al., 2009). We observed that shear stress, induced by medium flow over human pulmonary artery endothelial cells (HPAECs), caused a significant increase of PACSIN2 phosphorylation after 2–4 min of flow (Fig. 2D).

Phosphorylation directly influences the membrane binding of PACSIN2

We next examined the effect of phosphorylation on liposome binding by PACSIN2. Strikingly, the phospho-mimetic PACSIN2 mutants S313E, S373D and the S313E, S373D double mutant bound with reduced efficiency to liposomes made of Folch fraction lipids, a total brain lipid fraction that is enriched in negatively charged phosphatidylserine, as compared to WT PACSIN2 (Fig. 3A). Binding of PACSIN2 and the phospho-mimetic mutants to liposomes made of phosphatidylcholine (PtdCho) and phosphatidylethanolamine (PtdEtn) was greatly reduced compared to that of Folch liposomes (supplementary material Fig. S1A). Thus, PACSIN2 membrane binding appears to be dependent on the charge of the lipid.

Next, we examined the effect of PKC-mediated phosphorylation of PACSIN2 in HeLa cells (Fig. 3B). Overexpression of C-terminally GFP-tagged PACSIN2 induced cellular membrane tubules more efficiently than that of N-terminally GFP-tagged PACSIN2 (Fig. 1B). To activate PKC, we treated PACSIN2–GFP-expressing cells with the PKC activator PMA. Among the PMA-treated cells, the number of cells possessing PACSIN2-induced tubules was decreased, as compared to control cells (Fig. 3B,C). Overexpression of the phospho-mimetic S313E mutant also led to reduced membrane tubulation, as compared to WT PACSIN. However, in cells overexpressing the phosphorylation-deficient mutant S313A or the phospho-mimetic S313E mutant, PMA treatment did not influence membrane tubulation or PACSIN2–GFP

Journal of Cell Science (2015) 128, 2766-2780 doi:10.1242/jcs.167775

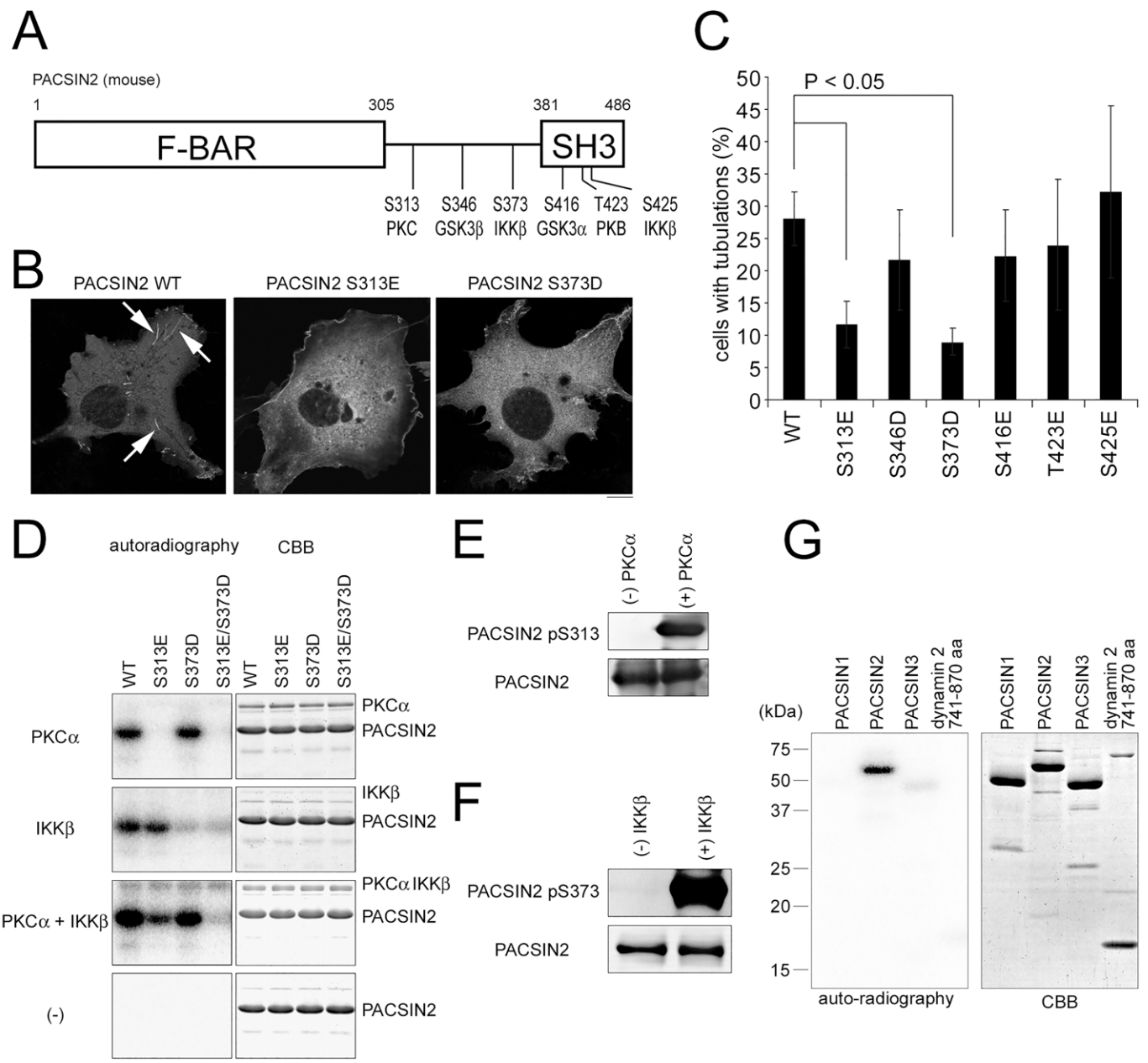

Fig. 1. PKC phosphorylates PACSIN2 at position S313. (A) Schematic representation of the domain architecture and predicted phosphorylation sites of PACSIN2. Amino acid residue numbers are indicated. (B) Representative confocal micrographs showing GFP fluorescence of HeLa cells overexpressing N-terminally tagged PACSIN2, PACSIN2 S313E, or PACSIN2 S373D. Note the tubular localization of PACSIN2 (arrows). Scale bar: 10 µm. (C) Quantification of cells overexpressing the indicated PACSIN2 mutants and containing at least one PACSIN2 tubule. Experiments were repeated three times, and 100 cells were counted in each experiment. Results are mean±s.d., $P<0.05$ by Student's *t*-test. (D) *In vitro* kinase assays. Purified full-length PACSIN2 WT and mutants were incubated with PKCα and/or IKKβ and [γ-^{32}P]ATP for 1 h at 30°C. The proteins were separated by SDS-PAGE, and phosphorylation was analyzed by autoradiography (left panel) and protein levels were assessed by staining with CBB (right panel). (E) Purified PACSIN2 was incubated with or without PKC in kinase buffer and analyzed by western blotting, using a phosphorylation-specific antibody against PACSIN2 phosphorylated at position S313 (PACSIN2 pS313) or an anti-PACSIN2 antibody. (F) Western blotting was performed as in E, but with IKKβ and an antibody against PACSIN2 phosphorylated at position S373 (PACSIN2 pS373). (G) *In vitro* kinase assays. Purified full-length PACSIN1, PACSIN2, PACSIN3 and the dynamin 2 PRD (amino acids 741–870) were incubated with PKCα and [γ-^{32}P]ATP for 1 h at 30°C, and analyzed as in D. We found that 0.80±0.19 (n=3) phosphates were incorporated within each PACSIN2 molecule, indicating that S313 is a unique PKCα phosphorylation site.

localization substantially. In cells overexpressing WT PACSIN2, PMA treatment promoted the phosphorylation of overexpressed WT PACSIN2 at S313, and treatment with the PKC inhibitor BIM reduced its phosphorylation, as observed by western blotting using an anti-phosphorylated-S313 antibody (Fig. 3D). To confirm the reduced affinity of phosphorylated PACSIN2 for membrane tubules, we examined the localization of the overexpressed S313E mutant, through its GFP tag, and of endogenous PACSIN2 by antibody staining in HeLa cells. Whereas endogenous PACSIN2 was observed in tubular structures, the S313E mutant did not extensively colocalize with these structures (supplementary material Fig. S1B). These results suggest that the loss of PACSIN2-containing membrane tubules by PKC activation is mediated by the phosphorylation of PACSIN2 at S313.

Journal of Cell Science (2015) 128, 2766-2780 doi:10.1242/jcs.167775

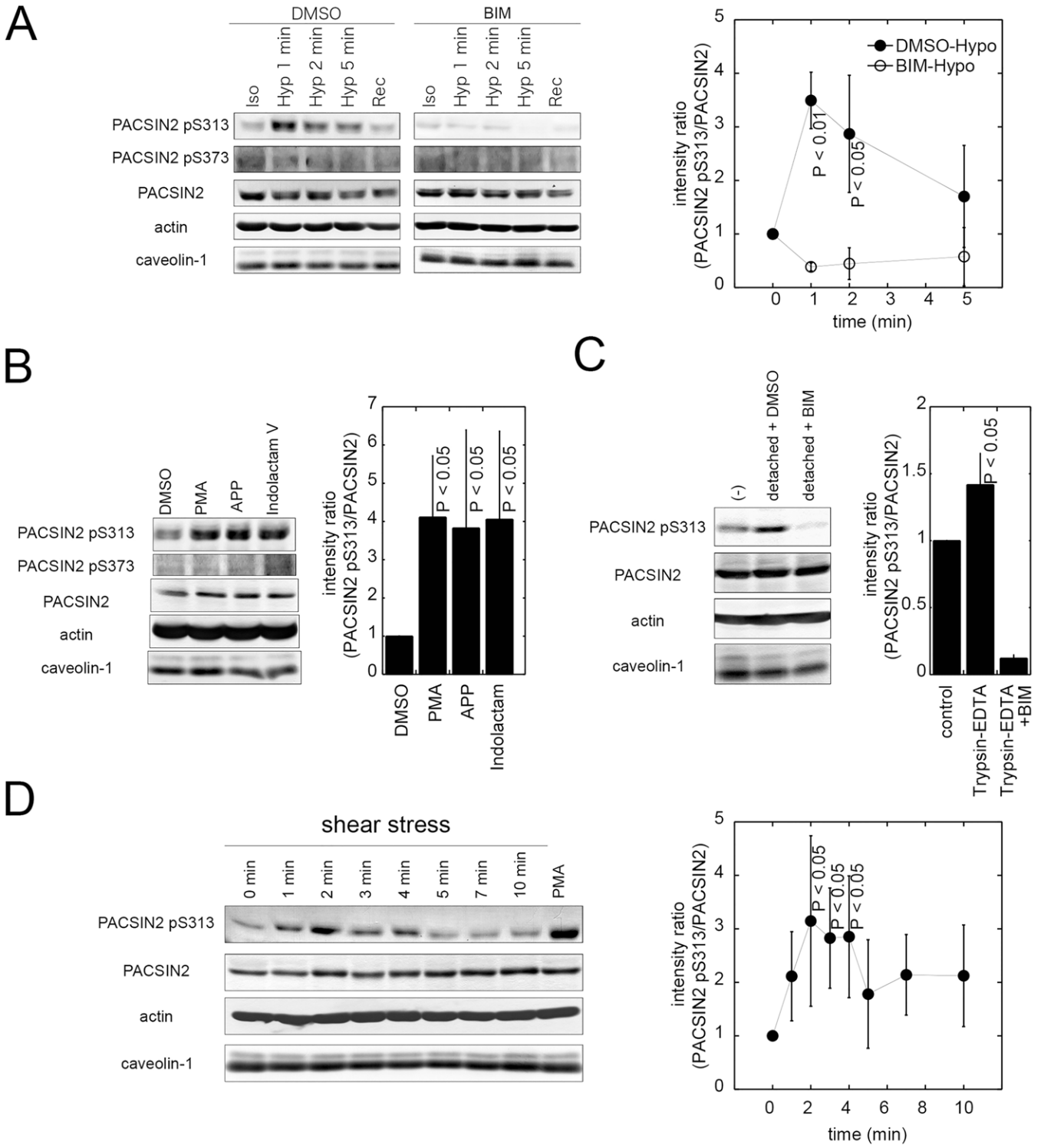

Fig. 2. PKC phosphorylates PACSIN2 at position S313 in cells. (A) Phosphorylation of PACSIN2 at S313 upon hypotonic treatment. HeLa cells were treated with 300 mOsm isotonic normal medium (Iso) or 30 mOsm hypotonic medium (Hyp) for the indicated times, in the presence of BIM or vehicle control (DMSO). Cells were harvested and then analyzed by western blotting, using antibodies against PACSIN2 phosphorylated at position S313 or S373 (pS313-PACSIN2 or pS373-PACSIN2, respectively), PACSIN2, actin and caveolin-1. After 5 min of treatment with hypotonic medium, the cells were allowed to recover by the application of normal 300 mOsm medium for 5 min (Rec). The intensity ratios of the western blotting signals obtained with the anti-pS313-PACSIN2 antibody over the anti-PACSIN2 antibody are plotted on the right (mean±s.d., *n*=3). (B) Phosphorylation of PACSIN2 at S313 upon PKC activation. HeLa cells were treated with the PKC activators PMA, APP or indolactam V, or with vehicle control (DMSO) for 5 min under isotonic conditions, and analyzed as in A. The intensity ratios of the western blotting signals with the anti-pS313-PACSIN2 antibody over the anti-PACSIN2 antibody are shown in the bar graph on the right (mean±s.d., *n*=4). (C) Phosphorylation of PACSIN2 in HeLa cells upon detachment from the substratum, in the presence of the PKC inhibitor BIM or vehicle control (DMSO). Non-detached cells served as a control (–). The intensity ratios are shown as in B (mean±s.d., *n*=4). (D) Phosphorylation of PACSIN2 upon shear stress. Human pulmonary artery endothelial cells were subjected to a flow of 15 dyn/cm^2 for the indicated times and analyzed as in A. PMA was used as a positive control. The intensity ratios are shown as in A (mean±s.d., *n*=4). All *P*-values were calculated with a Student's *t*-test.

Journal of Cell Science (2015) 128, 2766-2780 doi:10.1242/jcs.167775

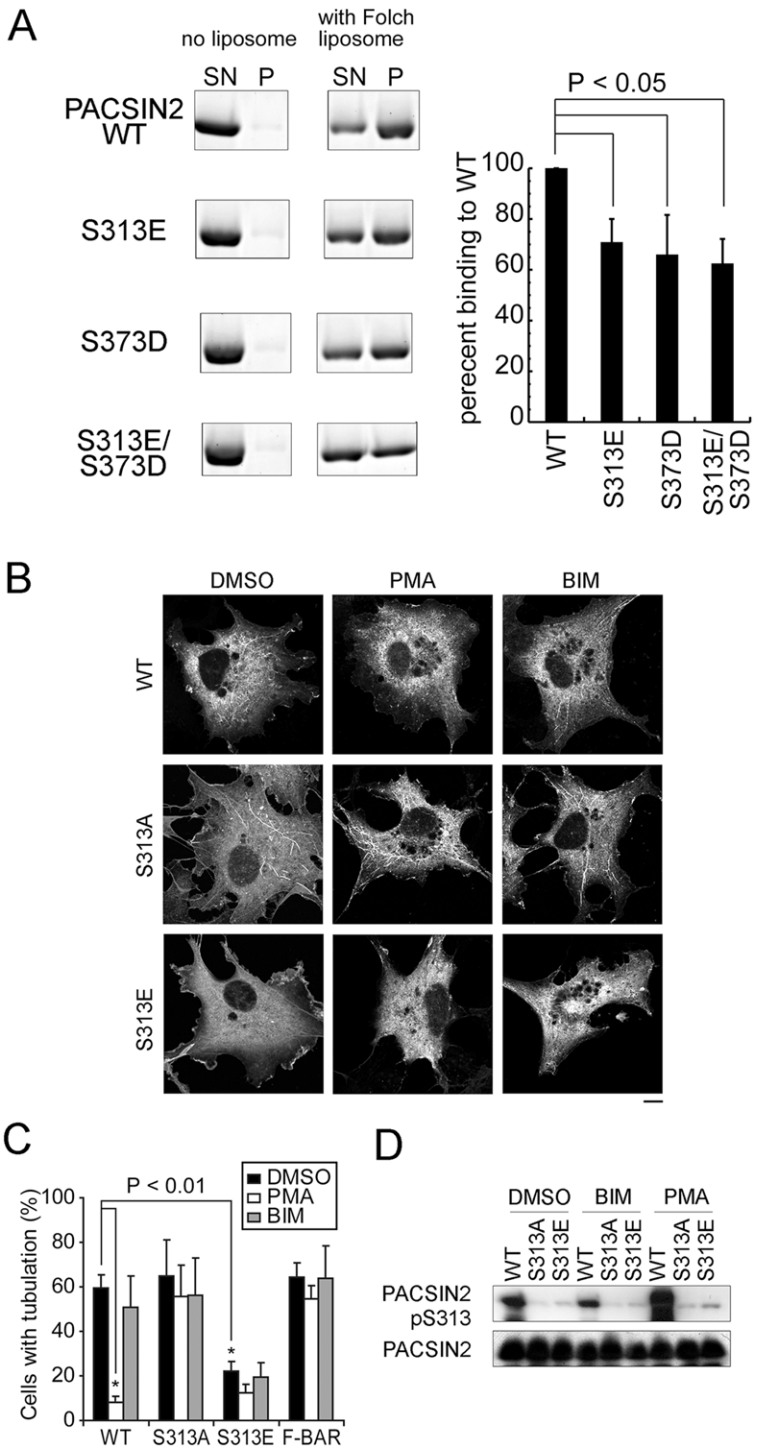

Fig. 3. Phosphorylated PACSIN2 shows reduced membrane affinity. (A) PACSIN2 binding to liposomes made of Folch fraction lipids, a total lipid fraction from brain. Purified PACSIN2, PACSIN2 S313E, PACSIN2 S373D and PACSIN2 S313E/S373D (2 µM) were each incubated with 1 mg/ml Folch liposomes and subjected to ultracentrifugation. The supernatant (SN) and pellet (P) were analyzed by SDS-PAGE and CBB staining. The percentage binding relative to PACSIN2 is shown are mean±s.d. (n=3), as quantified by the ImageJ software. P<0.05 by Student's t-test. (B) Representative images of HeLa cells overexpressing C-terminally GFP-tagged WT PACSIN2, the phospho-deficient mutant S313A or the phosphor-mimetic mutant S313E. Cells were treated with vehicle control (DMSO), PKC activator PMA (100 nM), or PKC inhibitor BIM (1 µM) for 30 min, and observed by confocal microscopy. Scale bar: 10 µm. (C) The numbers of cells containing at least one PACSIN2-induced tubule were counted, and presented as mean±s.d. (n=3, 100 cells were counted in each experiment). P<0.01 by Student's t-test. Note that C-terminally GFP-tagged PACSIN2 induced membrane tubulation more efficiently than N-terminally GFP-tagged PACSIN2 (compare Fig. 1B,C). (D) HeLa cells overexpressing WT PACSIN2, S313A, or S313E were treated with vehicle control (DMSO), BIM or PMA. The PKC-dependent phosphorylation of PACSIN2 was then examined by western blotting, using an antibody against PACSIN2 phosphorylated at position S313 (pS313).

Next, we analyzed the effect of S313 phosphorylation on the assembly of PACSIN2. F-BAR domains typically exist as dimers in solution (Shimada et al., 2007). To determine whether phosphorylation affects dimerization, analytical ultracentrifugation (AUC) experiments were performed. In these experiments, both PACSIN2 and the S313E mutant indistinguishably formed concentration-independent dimers (Fig. 4A). These data indicate that PACSIN2 phosphorylation does not affect the dimerization equilibrium in the analyzed concentration range.

It has been suggested that PACSIN2 is auto-inhibited by an interaction of its F-BAR and SH3 domains (Plomann et al., 2010; Shimada et al., 2010). To determine whether phosphorylation affected the auto-inhibition, we compared the assembly and the structures of PACSIN2 and the S313E mutant. In the X-ray structures of full-length PACSIN2 and the S313E mutant, the electron densities of the SH3 domains and the phosphorylation sites were not resolved (data not shown). We therefore utilized small angle X-ray scattering (SAXS) experiments to obtain structural information about PACSIN2 and the S313E mutant in solution. No significant differences in the scattering curves of PACSIN2 and the S313E mutant were apparent (Fig. 4B). The differences in the scattering curves between PACSIN2 and the isolated F-BAR

Journal of Cell Science (2015) 128, 2766-2780 doi:10.1242/jcs.167775

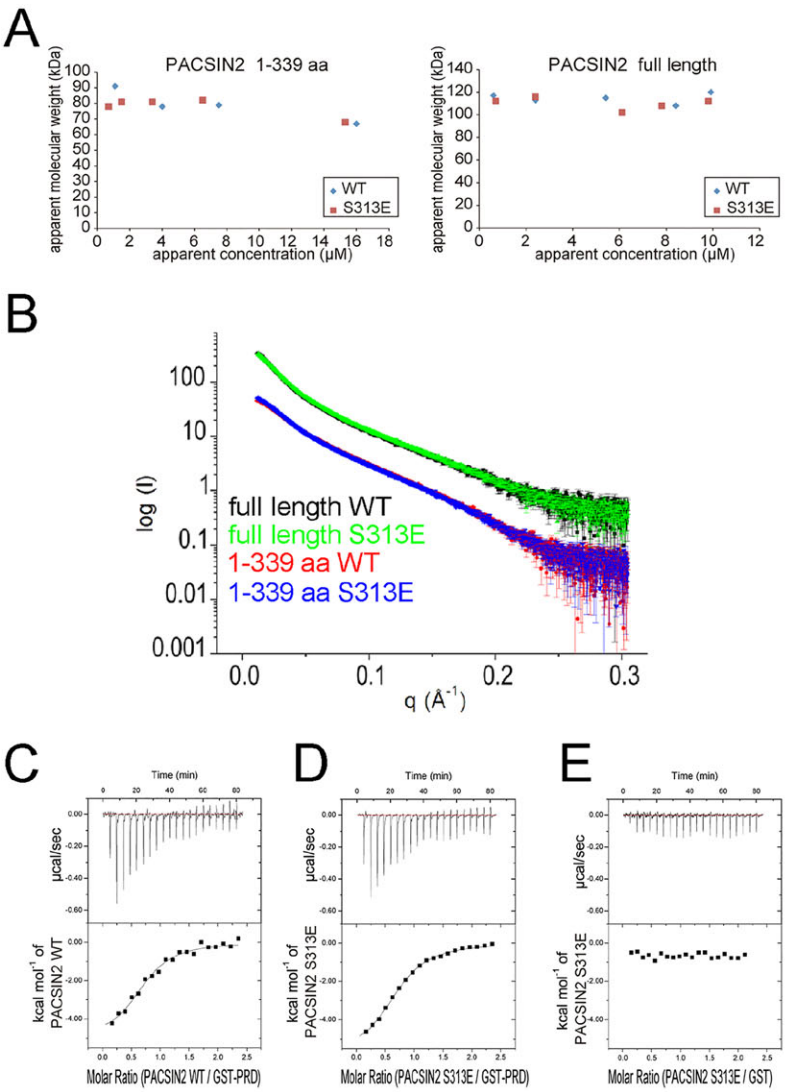

F

	PACSIN2 WT	PACSIN2 S313E
N	0.72±0.04	0.72±0.02
Kd (μM)	11±3	13±1

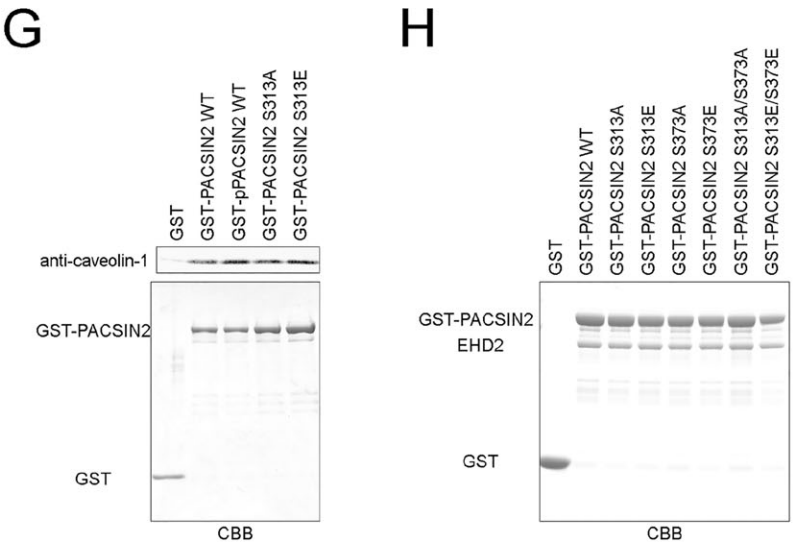

Fig. 4. *In vitro* assays of PACSIN2. (A) Analytical ultracentrifugation sedimentation equilibrium experiments were performed for different concentrations of PACSIN2 and a PACSIN2 construct without the SH3 domain (PACSIN2 1–339), in the absence or presence of the S313E mutation. The apparent molecular masses of the samples were determined at each concentration. All samples formed dimers throughout the concentration range tested. (B) SAXS data were obtained for PACSIN2 and its fragment without the SH3 domain (amino acids 1–339), in the absence or presence of the S313E mutation. The scattering curves of the wild-type (WT) protein and the S313E mutant superposed perfectly, indicating that the S313E mutation does not induce major conformational changes in PACSIN2. (C–F) The interaction of PACSIN2 with the PRD of dynamin 2 was examined by isothermal titration calorimetry (ITC). Solutions containing 1 mM PACSIN2 (C) or PACSIN2 S313E (D, E) were injected stepwise into the reaction cell containing 90 μM GST–PRD (C,D) or 90 μM GST (E), and the resulting heat changes were monitored. The upper panel shows the heating power as a function of time. The lower panel shows the integrated heating power normalized to the concentration of injected PACSIN2. The data were fitted using a single binding site model. From the fit, the binding stoichiometry (N) and the dissociation constant (K_d) were derived (F). Errors are standard errors of the fit. The observed sub-stoichiometric binding of PACSIN2 to the PRD of dynamin might be explained by the instability of the GST–PRD construct, which tended to precipitate and degrade to some extent. (G) Interactions of PACSIN2 with caveolin-1. GST pulldown experiments were performed to examine the interactions between caveolin-1 (amino acids 1–100, corresponding to the N-terminal cytoplasmic domain) at a concentration of 3 μM and different GST–PACSIN2 constructs. Upper panel, co-precipitated caveolin-1 was detected by western blotting. Lower panel, the input GST constructs were stained with CBB. The cytoplasmic domain of caveolin-1 was previously shown to bind PACSIN2 (Senju et al., 2011). (H) Interactions of PACSIN2 with EHD2. GST pulldown experiments were performed to examine the interaction between EHD2 (5 μM) and GST–PACSIN2, or the S313A, S313E, S373A, S373D, S313A/S373A or S313E/S373D mutants. The bound proteins were analyzed by SDS-PAGE followed by CBB staining.

Journal of Cell Science (2015) 128, 2766-2780 doi:10.1242/jcs.167775

fragment indicated the presence of additional electron density in PACSIN2, corresponding to the linker and the SH3 domain. However, we were not able to determine the exact position of the SH3 domain by either rigid body methods or *ab initio* modeling. Taken together, these data indicate that the conformation of PACSIN2 in solution is not altered by phosphorylation, thus strongly suggesting that the auto-inhibition of PACSIN2 is not affected by the phosphorylation.

We next tested whether phosphorylation affects the interactions of PACSIN2 with known binding partners, such as dynamin 2, EHD2 and caveolin-1. In isothermal titration calorimetry (ITC) experiments, both PACSIN2 and the S313E mutant bound at similar levels to the PRD of dynamin 2 (Fig. 4C–F). We also did not detect any differences in the affinity to dynamin 2 in co-immunoprecipitation experiments from cell extracts (data not shown). Furthermore, in pulldown and sedimentation assays, PACSIN2 and the S313E mutant bound similarly to caveolin-1 and EHD2, respectively (Fig. 4G,H). These data suggest that phosphorylation directly affects the membrane-binding ability of PACSIN2, but does not influence other molecular interactions.

Loss of membrane binding by PACSIN2 removes caveolae from the plasma membrane

For a long time, caveolae were thought to be long-lived steady-state plasma membrane structures (Hill et al., 2008; Pelkmans et al., 2004). However, recent studies with better time resolution have revealed that the lifetime of caveolae at the plasma membrane is shorter than expected, and varies depending on the cell cycle progression (Boucrot et al., 2011; Mohan et al., 2015). To examine the physiological effect of reduced PACSIN2 membrane binding, we tracked a stably expressing caveolin-1–DsRed-monomer (DsRedm) construct, as a marker of caveolae at the plasma membrane, using TIRF microscopy (Boucrot et al., 2011; Mohan et al., 2015; Pelkmans and Zerial, 2005). The amount of stably expressed caveolin-1–DsRedm was ∼25% of that of the endogenous caveolin 1 protein, as assessed by western blotting (supplementary material Fig. S1C), which is similar to results in previous functional studies (Mohan et al., 2015). We determined the coordinates of the center of the caveolin-1–DsRedm spots in each time-lapse image, and linked the coordinates of one image to the coordinates of the next image (supplementary material Fig. S2). The resulting sequence of coordinates can be used to detect the tracking duration, the velocity at each time point, and the fluorescence intensity of the proteins (Jaqaman et al., 2008). Although tracking durations might not be suitable for estimating the lifetime of caveolae, especially under kiss-and-run cycles (Pelkmans and Zerial, 2005), the tracking duration is thought to be correlated with the lifetime of caveolae, especially of those with longer tracking durations (Boucrot et al., 2011).

When we tracked caveolin-1 for 300 s, we found that a fraction of caveolae (∼10%) comprised stable structures at the plasma membrane, with tracking durations longer than 100 s (long-tracked caveolae); these could be observed as lines of caveolin-1–DsRedm in the kymographs (Fig. 5). However, the majority of caveolae had tracking durations below 100 s (Boucrot et al., 2011; Mohan et al., 2015) (Fig. 5A,I; supplementary material Movie 1). In cells treated with PACSIN2 small interfering RNA (siRNA), the fraction of long-lived caveolae was decreased (Fig. 5B,I; supplementary material Movie 1). To confirm the relationships between the levels of PACSIN2 at caveolae and longer persistence of caveolae on the plasma membrane, we expressed siRNA-resistant PACSIN2–GFP in PACSIN2-knockdown cells to quantify the amount of PACSIN2 at each observed caveola. The expression level of PACSIN2–GFP was approximately two times higher than that of endogenous PACSIN2 (supplementary material Fig. S1D). Interestingly, caveolae with longer tracking durations contained higher levels of PACSIN2 (Fig. 5C,H). Expression of PACSIN2–GFP in the PACSIN2-siRNA-treated cells restored the number of long-lived caveolae, confirming the functionality of PACSIN2–GFP (Fig. 5C,I; supplementary material Movie 2). An even larger decrease in long-lived caveolae was detected when a PACSIN2 mutant defective in membrane binding (R50D) was expressed in PACSIN2-siRNA-treated cells (Fig. 5D,I; supplementary material Movie 2), indicating that the R50D construct has a dominant-negative effect. Importantly, a decrease in the fraction of long-lived caveolae was also observed in cells expressing the S313E mutant of PACSIN2 (Fig. 5E,I; supplementary material Movie 2).

We then treated cells with the PKC activator PMA and examined the behavior of caveolae. PMA treatment under isotonic conditions led to a decrease in the number of caveolae (Fig. 5F,G; supplementary material Movie 3). After 300 s recording, especially the population of caveolae with tracking durations longer than 100 s was decreased (Fig. 5I). To confirm our observations on PMA treatment, we utilized Flp-in T-REx HeLa cells expressing caveolin-1–GFP (Mohan et al., 2015). The behavior of caveolin-1 upon PMA treatment was similar to that of cells stably expressing caveolin-1–DsRedm (supplementary material Fig. S3 and Movie 7). Interestingly, expression of the R50D, but not of the S313E mutant increased the diffusion coefficient of caveolin-1 spots under TIRF (Fig. 5J), reflecting the severity of the mutations for membrane binding (Shimada et al., 2010) (Fig. 3A). The diffusion coefficient of caveolae was also increased by PMA treatment, which induces the phosphorylation of various proteins including PACSIN2. These observations suggest that a decrease in PACSIN2 membrane binding by phosphorylation results in the removal of caveolae from the plasma membrane, in particular of the long-lived population.

The tracking duration of caveolae upon hypotonic treatment of cells

We next explored caveolar behavior in HeLa cells upon physiological activation of PKC by hypotonic treatment, using TIRF microscopy (Fig. 6; supplementary material Movies 4–6). The total number of caveolin-1 spots decreased after hypotonic treatment in a time-dependent manner, which correlated with the phosphorylation of PACSIN2 (Fig. 2A; Fig. 6A,B). Especially, the percentage of caveolae with longer tracking durations decreased upon hypotonic treatment, similar to the effect of the PMA treatment under isotonic conditions (Fig. 6E). In addition, the diffusion coefficient of caveolae was significantly increased by the hypotonic treatment (Fig. 6F).

We then tested the role of PKC for the hypotonicity-induced decrease of the caveolar-tracking durations at the plasma membrane. When PKC was inhibited by BIM under hypotonic conditions, the population of caveolae with longer tracking durations still showed a tendency to decrease (Fig. 6B,C,E), although BIM treatment suppressed phosphorylation of PACSIN2 (Fig. 2A). Furthermore, expression of WT PACSIN2 did not prevent the decrease in total caveolae number upon hypotonic treatment (Fig. 6B). However, the decrease in the percentage of caveolae that could be tracked for longer upon hypotonic treatment could be partially restored by overexpression of WT PACSIN2, although the number of total long-lived caveolae was decreased (Fig. 6D,E). Because longer-tracked caveolae had larger amount of PACSIN2, these results suggest that the amount of PACSIN2 at caveolae is crucial to mediating their persistence at the plasma membrane.

Journal of Cell Science

Journal of Cell Science (2015) 128, 2766-2780 doi:10.1242/jcs.167775

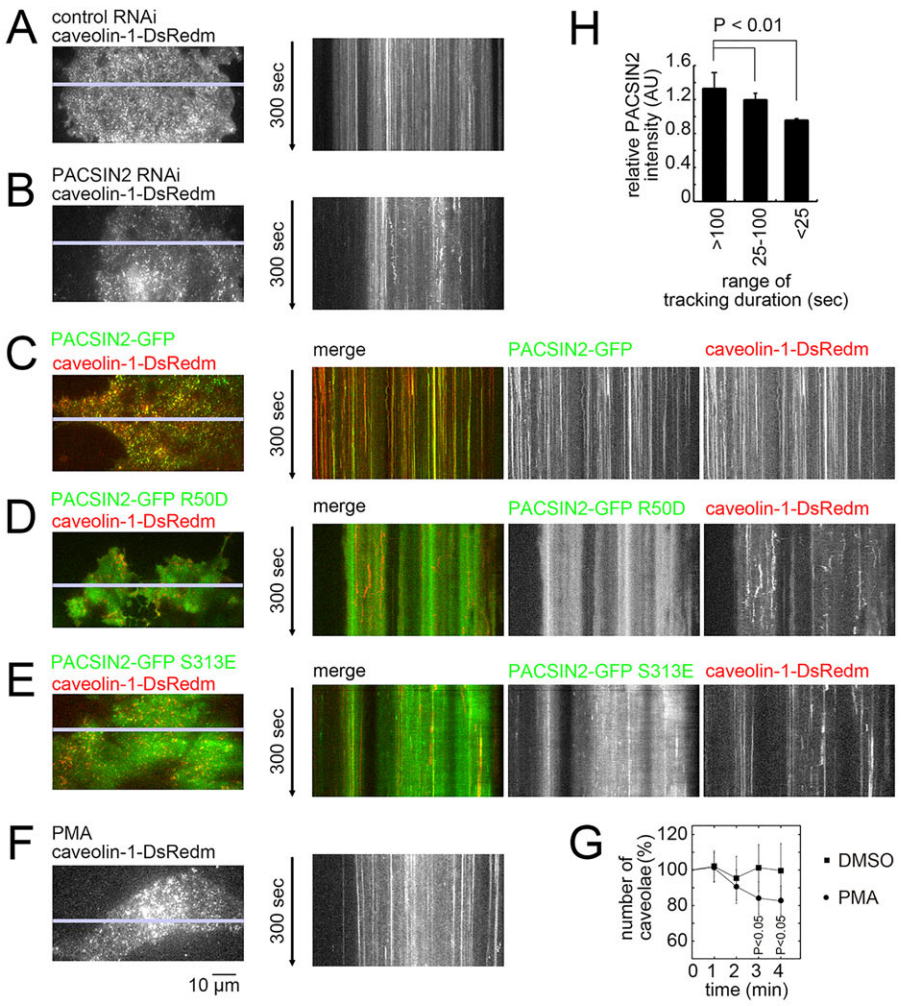

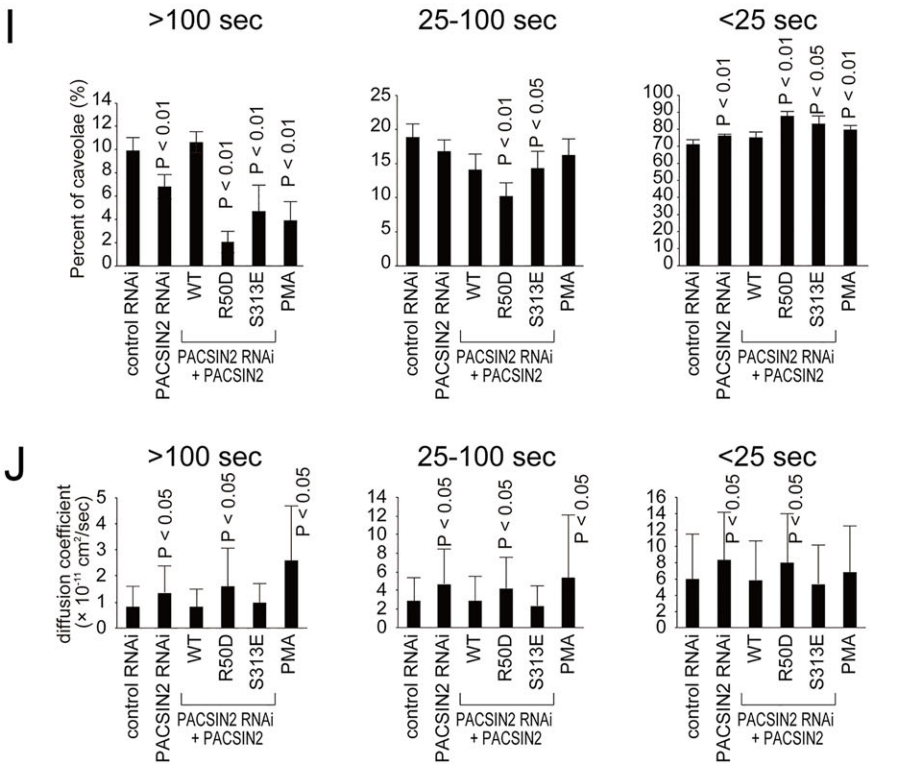

Fig. 5. PACSIN2 depletion causes shorter tracking durations of caveolae at the plasma membrane. (A,B) The fluorescence of stably transfected caveolin-1–DsRedm was monitored in cells treated with control siRNA or the siRNA for PACSIN2, using TIRF microscopy. The kymograph over 300 s was generated from the indicated line. Dotted vertical lines in kymographs indicate that caveolae could be tracked for shorter durations. (C–E) Stably transfected caveolin-1–DsRedm and GFP was monitored in cells overexpressing PACSIN2–GFP WT, PACSIN2–GFP R50D, or PACSIN2–GFP S313E, respectively, as in A and B. (F) Stably transfected Caveolin-1–DsRedm fluorescence was monitored in cells treated with PMA, after 1 min of the treatment, as in A and B. (G) Time courses following the number of distinct caveolin-1–DsRedm spots in HeLa cells under DMSO or PMA treatment by TIRF microscopy as in F. The number of caveolin-1–DsRedm spots were counted for each image, averaged for a 1 min interval, and shown as a percentage to the number of spots at the 0 min of the recording (mean±s.d., n=4–8). P values compared with 0 min were calculated with a Student's t-test. (H) The fluorescent intensities of PACSIN2 on caveolin-1–DsRedm spots. The fluorescent intensities of PACSIN2 on caveolin-1–DsRedm spots were measured, normalized for each cell, and classified according to the tracking durations of caveolin-1 spots (mean±s.d., n=6). P-values calculated with a Student's t-test are shown. (I) Quantification of tracking durations of caveolin-1–DsRedm spots from living cells by TIRF microscopy during 300 s of observation (mean±s.d., n=4–6). P-values compared to control siRNA-treated cells were calculated with a Student's t-test. (J) Quantification of diffusion coefficients of caveolin-1-DsRedm spots from living cells by TIRF microscopy during 300 s of observation (mean±s.d., n=4–6). P-values compared to control siRNA-treated cells were calculated with a Student's t-test.

Journal of Cell Science (2015) 128, 2766-2780 doi:10.1242/jcs.167775

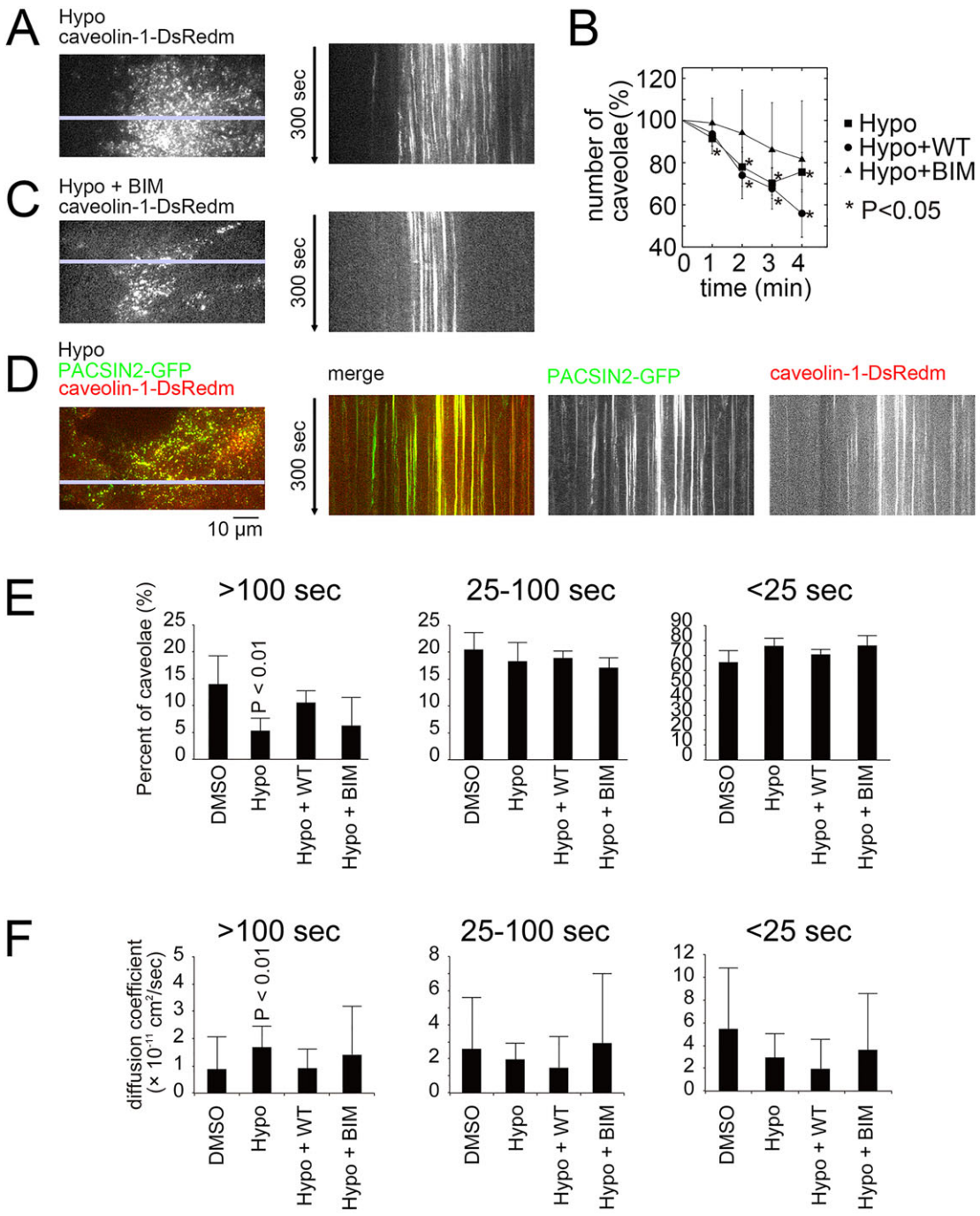

Fig. 6. Hypo-osmotic treatment destabilizes caveolae. (A,C,D) TIRF images of HeLa cells expressing caveolin-1 and PACSIN2. HeLa cells stably expressing caveolin-1–DsRedm were treated with hypotonic medium (Hypo) in the presence or absence of BIM (C) or control DMSO (A). PACSIN2 was co-expressed in (D). The images are representative for at least three independent experiments. The kymograph is from 1 min after hypotonic treatment during 300 s. (B) Time courses following the number of distinct caveolin-1–DsRedm spots in HeLa cells under hypotonic treatment by TIRF microscopy as in Fig. 5G. Shown are mean±s.d. (n=3–6). *P<0.05 compared to the 0 min value were calculated by Student's t-test. (E) Quantification of tracking durations of caveolin-1–DsRedm spots from live cells by TIRF microscopy during 300 s of observation after 1 min of hypotonic treatment (mean±s.d., n=3–6). P-values compared to DMSO-treated cells were calculated with a Student's t-test. (F) Quantification of diffusion coefficients of caveolin-1–DsRedm spots from living cells by TIRF microscopy during 300 s of observation after 1 min of hypotonic treatment(mean±s.d., n=3–6). P-values compared to DMSO-treated cells were calculated with a Student's t-test.

The time course of PACSIN2 localization and the effects of dynamin and EHD2

To dissect the function of PACSIN2 at caveolae, PACSIN2 localization to caveolae was monitored over time. PACSIN2 and caveolin-1 colocalized during the appearance and the disappearance of caveolae, as assessed by TIRF, strongly suggesting that PACSIN2 localizes to caveolae throughout their life at the plasma membrane (supplementary material Fig. S4).

Next, the relationship between PACSIN2 and dynamin 2 was examined. The S313E mutant of PACSIN2 still retained some residual membrane-binding affinity. We hypothesized that reduced membrane localization of the S313E mutant mimicking

Journal of Cell Science (2015) 128, 2766-2780 doi:10.1242/jcs.167775

phosphorylated PACSIN2 would not only be caused by reduced membrane binding but also by dynamin-dependent scission of PACSIN2-bound caveolae. Thus, WT PACSIN2- and PACSIN2-S313E-expressing cells were treated with the dynamin inhibitor dynasore, and the localization of PACSIN2 was examined. Strikingly, upon dynasore treatment, cells expressing WT PACSIN2 or the S313E mutant exhibited increased PACSIN2 membrane localization (Fig. 7A). In contrast, dynasore did not alter the membrane localization of the phosphorylation-deficient S313A mutant. This suggests that dynamin promotes the removal of the S313E mutant, and presumably of phosphorylated PACSIN2, from the plasma membrane.

To further examine the correlation between dynamin function and the partial removal of phosphorylated PACSIN2 from the membrane, we tracked PACSIN2 and dynamin 2 by TIRF, assuming that membrane-bound PACSIN2 was localizing to caveolae (Senju et al., 2011). The levels of dynamin 2 present on each PACSIN2 spot were examined (Fig. 7B,C), and we found that the decrease in PACSIN2 levels was associated with increasing amounts of dynamin 2. In particular, dynamin 2 levels at caveolae peaked when the levels of PACSIN2 were reduced to 50% of its maximum. These data suggest that the decreased levels of PACSIN2 at caveolae induced by phosphorylation allow dynamin-dependent membrane scission.

Finally, the relationship between PACSIN2 and EHD2 was examined. EHD2 is known to influence the stability of caveolae at the plasma membrane without affecting the formation of caveolae; its Eps15-homology domain has been reported to bind to NPF motifs in PACSIN2 (Moren et al., 2012; Stoeber et al., 2012). Therefore, we expressed EHD2–mCherry in control cells or in cells in which PACSIN2 was knocked down by siRNA, and examined the behavior of caveolae. The expression of EHD2 led to an increase in the percentage of long-tracked caveolae in PACSIN2-knockdown cells, but not in cells treated with a control siRNA (Fig. 8A-C, supplementary material Movie 8). Furthermore, expression of EHD2 in PACSIN2-knockdown cells reduced the caveolar diffusion coefficient back to control levels (Fig. 8D). This suggests that EHD2 and PACSIN2 cooperate to stabilize caveolae at the plasma membrane.

DISCUSSION

In this study, we identified S313 as the unique PKCα phosphorylation site in PACSIN2 (Fig. 1). PACSIN2 phosphorylation was observed after PKC activation by chemical compounds such as PMA, and this phosphorylation was suppressed by the PKC inhibitor BIM. Furthermore, PKC activation suppressed the membrane tubulation activity of PACSIN2 in cells (Fig. 3). Previous studies have suggested that the PMA-mediated activation of PKC affects the functions of caveolae, although the detailed dynamics upon PKC activation were unclear (Oka et al., 1997; Sharma et al., 2004; Smart et al., 1994, 1995). Our group and others have shown that PACSIN2 localizes to and functions at caveolae (Hansen et al., 2011; Koch et al., 2012; Senju et al., 2011). Moreover, BAR domain proteins are known to bind to negatively-charged lipids, including phosphatidylinositol 4,5-bisphosphate [PtdIns(4,5)P_2] (Suetsugu et al., 2014), and PtdIns(4,5)P_2 is enriched at caveolae (Fujita et al., 2009). S313 phosphorylation caused a decrease in the membrane-binding and tubulation abilities of PACSIN2. These effects are likely mediated by repulsion between the negative charge of phosphorylated S313 and the negatively charged lipid surfaces, given that we did not observe any effects of phosphorylation on the interactions with caveolin-1, dynamin 2 and EHD2, or on PACSIN2 dimerization (Figs 1 and 4). SAXS measurements of the S313E mutant, which is thought to mimic phosphorylation at S313, were identical to PACSIN2 WT, indicating that the conformation of PACSIN2 was not affected by the phosphorylation. However, it is still possible that the spatial organization of the binding partners, such as dynamin and EHD2, might be modified by phosphorylation. Taken together, our observations suggest that PACSIN2 phosphorylation leads to the dissociation of PACSIN2 from caveolae at the plasma membrane.

The expression of the S313E mutant of PACSIN2 reduced the tracking duration of caveolae at the plasma membrane. We found that the phosphorylation of PACSIN2 by PKC is induced by changes in membrane tension caused by mechanical stimuli, such as hypotonic and shear stresses (Fig. 2). The application of hypotonic stress also led to a reduction in caveolar-tracking durations (Fig. 6). This suggests that PACSIN2 might have mechano-sensitive properties. However, the application of the PKC inhibitor BIM

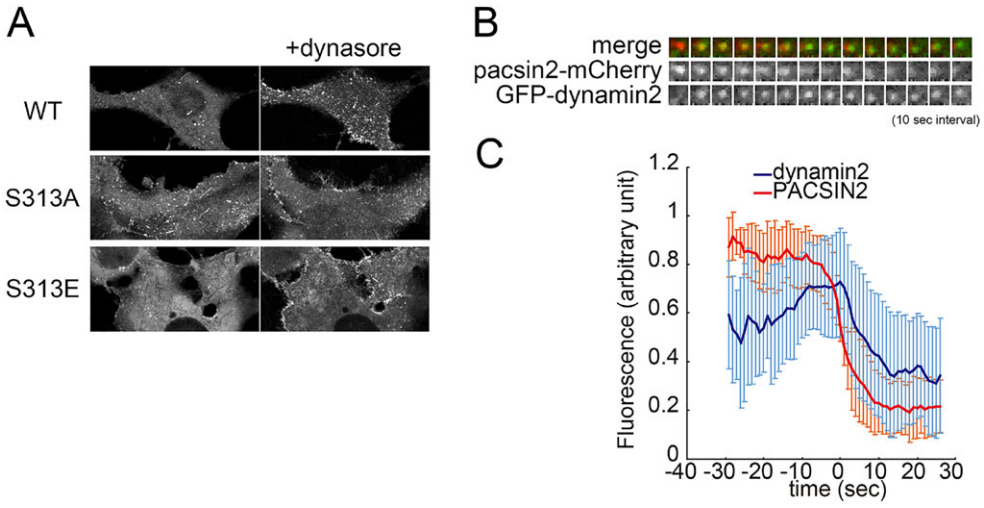

Fig. 7. Time courses of PACSIN2 and dynamin localizations. (A) Dynamin-dependent removal of PACSIN2 from the plasma membrane. HeLa cells overexpressing WT PACSIN2–GFP, or the S313A or S313E mutants were treated with the dynamin inhibitor dynasore. The same cells before and after 5 min treatment with dynasore (40 μM) were observed by confocal microscopy. The images are representatives of at least three independent experiments. (B,C) Time courses of the PACSIN2 and dynamin 2 localizations. (B) TIRF images of HeLa cells transfected with GFP–dynamin-2 (green) and PACSIN2–mCherry (red). Representative sequential images of disappearance of PACSIN2 are shown. (C) Quantification of the fluorescence intensity of dynamin 2 upon the disappearance of PACSIN2 (mean±s.d., *n*=69).

Journal of Cell Science (2015) 128, 2766-2780 doi:10.1242/jcs.167775

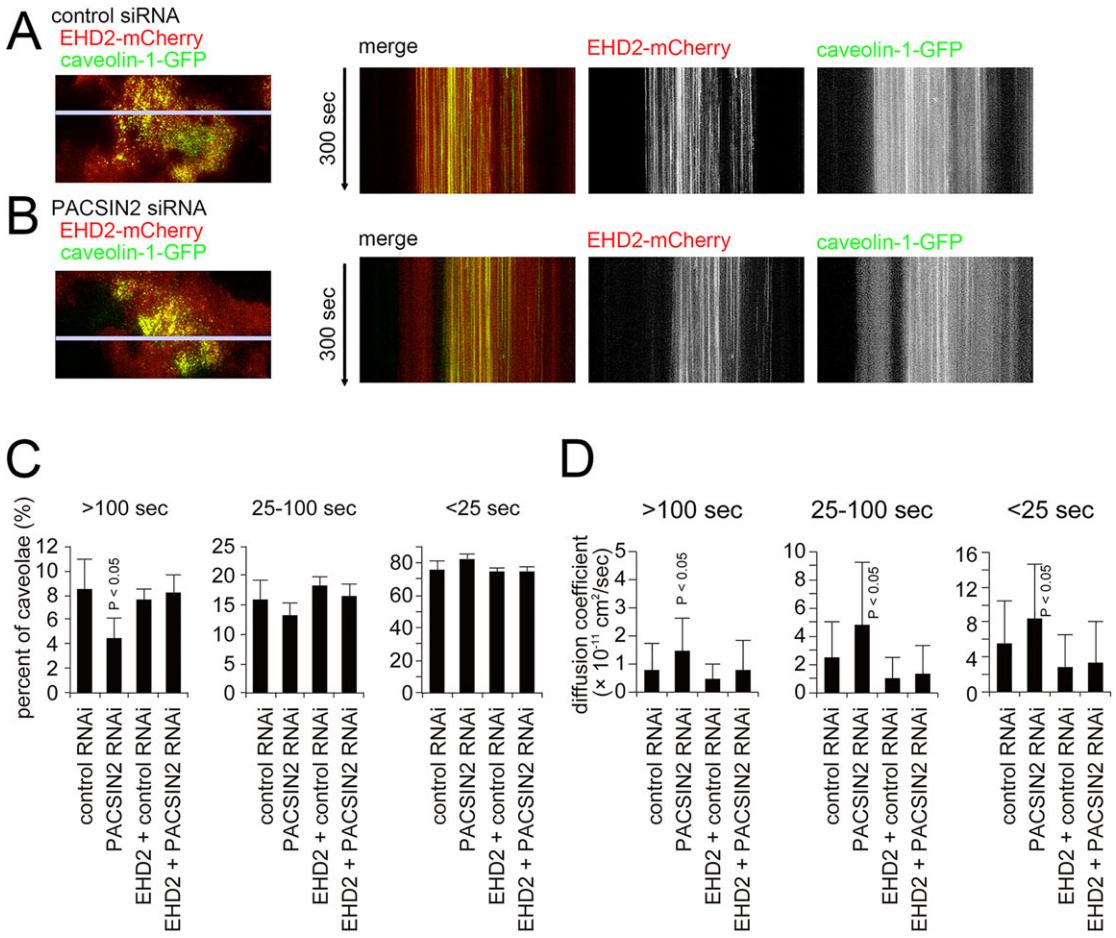

Fig. 8. The expression of EHD2 restores the effect of PACSIN2 downregulation. (A,B) Stably transfected caveolin-1–GFP was monitored in cells overexpressing EHD2–mCherry treated with (A) control or (B) PACSIN2 siRNA. (C) Quantification of tracking durations of caveolin-1–GFP spots by TIRF microscopy during 300 s of observation (mean±s.d., *n*=4). *P* values compared to control RNAi-treated cells were calculated by Student's *t*-test. (D) Quantification of diffusion coefficients of caveolin-1-GFP spots by TIRF microscopy during 300 s of observation (mean±s.d., *n*=4). *P* values compared to control RNAi-treated cells were calculated by Student's *t*-test.

did not completely prevent the shortening of the caveolar tracking duration caused by hypotonic treatment, although BIM suppressed PACSIN2 phosphorylation (Fig. 6). Hypotonic treatment is considered to induce various biochemical reactions in addition to the activation of PKC. Therefore, PACSIN2 phosphorylation is sufficient to reduce the tracking duration of caveolae at the plasma membrane, but it is not the only mechanism.

The disappearance of caveolin-1 from the plasma membrane, as judged by TIRF microscopy, can be explained by either the uptake of caveolae into the cell or the disassembly of caveolin-1 at the plasma membrane without endocytosis. We presently cannot distinguish between these two possibilities without observing the behavior of each caveolin-1 molecule with nanometer resolution. However, PACSIN2 was phosphorylated when caveolae became short-lived upon either PMA treatment or hypotonic stress. Therefore, we suggest that PACSIN2 plays an important role in maintaining caveolae in a long-lived state at the plasma membrane.

What might be the mechanism of PACSIN2-mediated maintenance of long-lived caveolae on the plasma membrane? In the absence of hypotonic stress, a reduction in caveolar-tracking duration was observed by expressing either the phospho-mimetic PACSIN2 mutant S313E or a PACSIN2 mutant deficient in membrane binding (Fig. 5). The RNAi-mediated knockdown of endogenous PACSIN2 also reduced caveolar tracking durations (Fig. 5). These observations suggest that the amount of unphosphorylated PACSIN2, and possibly that of its two paralogs PACSIN1 and PACSIN3, is crucial for maintaining long-lived caveolae at the plasma membrane. Consistent with this, overexpressed PACSIN2 colocalized with caveolae and increased the number of caveolae containing PACSIN2 (Senju et al., 2011). In addition, the levels of PACSIN2 were higher on caveolae that could be tracked for longer (Fig. 5H).

Our group and others have previously reported that PACSIN2 is involved in the morphogenesis of caveolae and the recruitment of dynamin to caveolae (Hansen et al., 2011; Koch et al., 2012; Senju et al., 2011). However, EHD2 also binds to PACSINs (Braun et al., 2005; Hansen et al., 2011; Moren et al., 2012; Stoeber et al., 2012) and is also involved in maintaining the stability, but not the formation, of caveolae. Our observations of caveolin-1 and PACSIN2 by TIRF confirmed that PACSIN2 localized to caveolae from their appearance to their disappearance (supplementary material Fig. S4). This is consistent with a role of PACSIN2 in caveolae morphogenesis and stability. Interestingly, the expression of EHD2 restored the decreased number of caveolae that could be tracked for longer induced by the decrease in the PACSIN2 levels back to normal levels (Fig. 8). We speculate that PACSIN2 functions by interacting with EHD2 at caveolae in order to maintain long-lived caveolae at the plasma membrane.

How can the stabilizing effect of PACSIN2 on caveolae be reversed to allow dynamin-mediated scission of caveolae? PACSIN2 binds to the SH3 domain of dynamin, a protein that promotes scission of invaginations, such as clathrin-coated pits and caveolae (Senju et al., 2011). The F-BAR domain proteins, including PACSIN2, are considered to form tightly packed helical alignments on the necks of invaginated membranes (Rao et al., 2010; Shimada et al., 2007). The tight packing of the tubules by the F-BAR domain PACSIN1 protein has been reported to stiffen the tubules (Ramesh et al., 2013), which might prevent dynamin from mediating membrane scission. Furthermore, PACSIN2-bound EHD2 might further protect the membrane invagination from scission. In this case, phosphorylation-mediated weakening of PACSIN2 binding to the membrane might loosen the tight packing of the F-BAR domain oligomers and provide the space for dynamin to cleave the membrane. In the case of hypotonic treatment, the observed decrease in caveolae number could not be inhibited by BIM treatment. This could possibly be due to mechanical forces at the plasma membrane following hypotonic treatment, which could loosen the packing of the F-BAR domains even of non-phosphorylated PACSIN2.

When we examined the dynamin recruitment, TIRF imaging indicated that more dynamin2 was recruited to the PACSIN2 spots shortly before PACSIN2 disappeared from the plasma membrane. At the same time, the observed kinetics support a role for PACSIN2 in dynamin 2 recruitment. The highest concentration of dynamin 2 coincided with a 50% decrease in PACSIN2 levels (Fig. 7C). This is in agreement with the idea that a decrease in the levels of PACSIN2 at the necks of caveolae is an important step before membrane scission and subsequent endocytosis of caveolae. Dynamin might be recruited to the neck of caveolae by PACSIN2, but it might not be able to cleave the membrane without the partial removal of PACSIN2 induced by phosphorylation.

Other caveolar components essential for caveolar integrity are the cavin proteins, which include four mammalian members (Hansen et al., 2013; Hill et al., 2008; Kovtun et al., 2014; Ludwig et al., 2013). Cavins have been shown to bind to and/or recruit PKCα (Gustincich et al., 1999; Hill et al., 2012; Izumi et al., 1997), and cavin-1 knockdown results in increased caveolar mobility (Hill et al., 2008). Furthermore, cavin-1 is known to interact with EHD2 (Moren et al., 2012). We therefore postulate that a PACSIN2–EHD2–cavin-1 complex could play an essential role in caveolar dynamics.

MATERIALS AND METHODS

Plasmid construction

Caveolin-1, PACSIN2, EHD2 and dynamin 2 constructs were prepared as described previously (Senju et al., 2011). FLAG–PKCα was prepared by subcloning the rabbit PKCα cDNA into the pCMV-Tag 2 vector (Stratagene) (Ono et al., 1988). Site-directed mutagenesis was performed using a QuikChange site-directed mutagenesis kit (Stratagene), according to the manufacturer's protocol. siRNA was prepared as described previously (Senju et al., 2011).

HeLa cell culture, transfection, and live imaging

HeLa cells were cultured as described previously (Senju et al., 2011). Flp-in T-REx HeLa cells were cultured in Dulbecco's modified Eagle's medium (DMEM) supplemented with 10% Tet System Approved fetal bovine serum (FBS), as described previously (Ditchfield et al., 2003; Mohan et al., 2015). For the hypotonic treatment, DMEM, supplemented with 10% fetal calf serum (FCS), was diluted 1:10 (Sinha et al., 2011). Phorbol 12-myristate 13-acetate [PMA, also known as 12-*O*-tetradecanoylphorbol-13-acetate (TPA)] (Sigma, P8139) (100 nM), δ-amyloid precursor protein modulator (APP, Santa Cruz Biotechnology, 204424) (100 nM), (−)-Indolactam V (Wako Pure Chemical Industries, 097-05911) (100 nM), and bisindolylmaleimide I, hydrochloride (BIM, Calbiochem, 203291) (1 μM) were each applied to the cells incubated in serum-free DMEM for 5 min. The cells were then lysed in SDS-PAGE sample buffer for western blot analyses. For the analysis of phosphorylation upon detachment, HeLa cells were washed with PBS, detached with trypsin and harvested in the presence of the PKC inhibitor BIM or vehicle control (DMSO).

Transfection was performed with the Lipofectamine LTX and PLUS reagents (Invitrogen) or the NEON transfection system (Invitrogen), according to the manufacturer's protocols, except that the caveolin-1-encoding expression plasmid was reduced to 0.1 μg per 3.5 cm dish in order to avoid excessively high overexpression. Then, cells stably expressing caveolin-1–GFP or –DsRed-Monomer were selected with G418. Cells with weaker expression were analyzed by TIRF microscopy, to ensure that the expression was equivalent to or less than that of endogenous caveolin-1 (supplementary material Fig. S1C). Mouse PACSIN2 was then transfected into cells along with the siRNA for PACSIN2 (Senju et al., 2011), and the cells were analyzed after 2 days. Mouse PACSIN2 was resistant to the siRNA targeted to human PACSIN2. For live observation by total internal reflection microscopy, HeLa cells were grown on a glass-bottomed dish, with DMEM containing 10% FBS and 10 mM HEPES (pH 7.5). The images were acquired for 5 min at 1 or 0.5 s intervals with a total-internal-reflection (TIRF) microscopy system connected to a confocal microscope (Olympus FV1000D), with a 100× NA 1.45 oil immersion objective (Olympus), a Cascade 2 CCD camera (Photometrics) and the MetaMorph software.

Tracking of caveolae

Caveolin-1 spots, which we assume to represent caveolae, were tracked for 300 s to obtain the frame number, the *x*-*y* coordinates, and the signal intensities of caveolin-1 and PACSIN2, using the programs developed by Jaqaman et al., run on the Matlab software (Mathworks) (Jaqaman et al., 2008). Image sequences that showed a significant focus drift were not used for the analysis. Briefly, the coordinates of the center of the fluorescent spot of each time-lapse TIRF image were estimated by Gaussian fitting, and the coordinates in each image were linked by the prediction of spot movement, under the assumption that the spots do not change their direction of movement randomly (i.e. the spots are supposed to move with inertia). A representative track overlaid on the fluorescent images is shown in supplementary material Fig. S2. The threshold for detecting spots was adjusted for each experiment. Several thousands of spots were detected during 300 s for each cell. The pixel values (fluorescent intensities) were examined from the coordinates. The diffusion coefficients of caveolae were calculated from the linked coordinates. The mean square displacement (MSD) was calculated for each caveola track, and the diffusion coefficient was determined from the slope of MSD over time of the approximation straight line passing through the origin by least square methods. A representative plot of the MSD is shown in supplementary material Fig. S2. The length of the sequence of the coordinates over time is the tracking duration.

Tracking of fluorescent intensities

Tracking of fluorescent intensities at appearance and disappearance was performed as described previously (Shimada et al., 2007). All images were processed with ImageJ (NIH) and Photoshop (Adobe). For each spot of caveolin-1 or PACSIN2 in the TIRF images, the fluorescence intensity was plotted over time. The fluorescence intensity was normalized between a maximum, set as 1, and minimum, set as 0, for each event of spot appearance and disappearance from the TIRF images. The mean and the standard deviations were calculated. The time at the half-maximum intensity of caveolin-1 or PACSIN2 was set to be 0.

Endothelial cell culture and shear stress experiments

Human pulmonary artery endothelial cells (HPAECs) were exposed to laminar shear stress with a parallel plate-type device, as described previously (Yamamoto et al., 2007). The intensity of the wall shear stress (τ, dynes/cm^2) on the cell layer was calculated by the formula $\tau=6Q/a^2b$,

where the cell layer was calculated as the perfusate (poise), Q is the flow volume (ml/s), and a and b are the cross-sectional dimensions of the flow path. All experiments were performed at 37°C in a CO_2 incubator. The cells were subjected to a flow of 15 dyn/cm^2 for the indicated times and analyzed. PMA was applied as a positive control.

Antibodies

The anti-PACSIN2 antibody was affinity purified from the serum of rabbits immunized with the F-BAR domain of PACSIN2 (Senju et al., 2011). The anti-PACSIN2 antibody from Abcam was also used for western blots. The anti-actin (MAB1501) antibody was purchased from Millipore, CA. The antibody against PACSIN2 phosphorylated at S313 was affinity purified from the serum of rabbits immunized with the PACSIN2 peptide CNRTL(pS)RREKK (pS, represents the phosphorylated serine; Hokkaido System Science, Sapporo, Japan) conjugated to Keyhole limpet hemocyanin (KLH) (Thermo Fisher Scientific Inc.). The antibody against PACSIN2 phosphorylated at S373 was affinity purified from the serum of rabbits immunized with the PACSIN2 peptide DDTGS(pS)ISEKEC (MBL International, Inc., Japan). The mouse monoclonal anti-caveolin-1 (7C8) and rabbit polyclonal anti-caveolin-1 antibodies were purchased from Santa Cruz Biotechnology and Cell Signaling Technology, respectively. The signals of western blotting were quantified by ImageJ (NIH, USA).

Recombinant proteins

Glutathione S-transferase (GST)–PACSIN2 (mouse), GST–PACSIN2-F-BAR domain (amino acids 1–339), GST-PACSIN1 (mouse), GST–PACSIN3 (mouse), GST–dynamin-2-PRD (amino acids 741–870), GST–caveolin-1 fragments (mouse) (amino acids 1–100) and GST–EHD2 were expressed in *Escherichia coli* (or *E. coli* DE3 Rosetta), as described previously (Daumke et al., 2007; Shimada et al., 2010). GST was removed with PreScission Protease (GE Healthcare). FLAG–PKCα was expressed in FreeStyle 293 cells, according to the manufacturer's protocol (Invitrogen). The protein was incubated with FLAG agarose (Sigma), and eluted with 0.1 mg/ml FLAG peptide in a buffer containing 50 mM Tris-HCl pH 7.5, 150 mM NaCl, and 50% glycerol. The IκB kinase (IKKβ) was obtained from Millipore, CA. The EHD2 protein was expressed and purified as described previously (Daumke et al., 2007).

In vitro kinase assays

In vitro kinase assays were performed as previously reported (Konishi et al., 1997). Purified PACSINs were incubated with FLAG-PKCα and/or IKKβ and [γ-^{32}P]ATP, in a reaction mixture containing 20 mM Tris-HCl pH 7.5, 10 mM $MgCl_2$, 1 mM ATP, 1 mM DTT, and 0.5 mM $CaCl_2$, for 1 h at 30°C. The proteins were separated by SDS-PAGE, and the phosphorylation was analyzed by autoradiography. Reactions without ATP were performed as negative controls.

Pulldown assays

Pulldown assays with the indicated fragments were performed in 20 mM Tris-HCl pH 7.5, 150 mM NaCl, 1 mM phenylmethylsulfonyl fluoride (PMSF), 10% glycerol, 5 mM EDTA, 1% Triton X-100 and the indicated protein concentrations. The purified proteins and glutathione Sepharose beads were mixed in the buffer for 1 h at 4°C. After washing, the bound proteins were visualized by western blotting or Coomassie Brilliant Blue (CBB) staining, after SDS-PAGE.

Small angle X-ray scattering measurements

SAXS data were collected at beamline P12 at PetraIII in Hamburg, Germany. Solutions of all four PACSIN2 constructs were measured at 3, 8 and 15 mg/ml, in 20 mM Tris-HCl pH 7.5 containing 150 mM NaCl. The initial data analysis was performed with the program Primus (Konarev et al., 2003). Radii of gyration (R_g) were obtained from Guinier fits in a data range where $q \times R_g < 1.3$. Theoretical scattering curves from PDB models were calculated with the program Crysol (Svergun et al., 1995). *Ab initio* shape determination was performed with the program Dammif (Franke and Svergun, 2009) by imposing two-fold symmetry. Twenty bead models were calculated for each construct. The models were averaged and filtered to obtain the most probable model. The program Situs (Wriggers, 2010) was used to compute a volumetric map from the most probable bead model and to fit the crystallographic models into the SAXS envelope. The combined *ab initio* and rigid body modeling approach was performed with the program Bunch (Petoukhov and Svergun, 2005). Scattering curves were plotted using the program Origin (Origin Labs), and structural figures were prepared with Pymol (Schrödinger) (DeLano Scientific; http://www.pymol.org).

Analytical ultracentrifugation

Sedimentation equilibrium runs were performed in 20 mM Tris-HCl buffer pH 7.5, containing 150 mM NaCl and 2 mM DTT, in an XL-I analytical ultracentrifuge (Beckmann) using six-channel centerpieces with an optical path length of 12 mm. Sample volumes of 100 µl were analyzed at 10,000, 15,000 and 20,000 rpm, by monitoring the absorbance at 280 nm. The apparent molecular mass at each protein concentration was determined by fitting the data from the three speeds simultaneously, using the program Sedphat (Schuck, 2003).

Liposome co-sedimentation assay

The liposomes contained PtdCho and PtdEtn (7:3 mass ratio) (Sigma Aldrich) or the Folch fraction, a brain total lipid fraction rich in phosphatidylserine (PtdSer) (Folch et al., 1957; Michelsen et al., 1995) (Avanti Polar Lipids). The lipids were first dissolved in chloroform and methanol (1:1) for PtdCho and PtdEtn or in chloroform for the Folch fraction. The lipids were mixed and dried under nitrogen gas, followed by under vacuum. The dried lipids were re-suspended in buffer containing 25 mM Hepes pH 7.4 and 150 mM NaCl to form liposomes for 1 h at 37°C. The protein (2 µM) and liposomes (1 µg/µl) were mixed. After a 30-min incubation at room temperature, the liposomes were precipitated by centrifugation at 100,000 ***g*** for 30 min in a TLA100 rotor (Beckman Coulter). The pellet and supernatant were examined by SDS-PAGE, and visualized by SimplyBlue SafeStain (Invitrogen) or CBB staining. Representative data from three independent experiments are shown in the figure.

Isothermal titration calorimetry

ITC experiments were performed at 10°C in an ITC200 device (MicroCal, Piscataway, NJ), using the indicated protein concentrations in a buffer containing 20 mM Tris-HCl pH 7.5, 150 mM NaCl, and 2 mM DTT. Binding isotherms were fitted, and equilibrium dissociation constants were calculated using the MicroCal ORIGIN software.

Statistical analysis

All statistical analyses were performed using the Microsoft Excel software. Significance was assessed by the Student's *t*-test. All images are representative of at least three independent experiments.

Acknowledgements

We would like to thank Naoaki Saito (Kobe University, Japan) and Shigeo Ohno (Yokohama City University) for the PKCα construct, and Alexis Gautreau (CNRS, France) for critical reading of this manuscript, and Richard Lundmark (Umea University, Sweden) and Stephen Taylor (Cancer Research UK) for the FLP-IN T-Rex HeLa cells expressing caveolin-1–GFP. We also would like to thank Marcel Jurk (FMP, Berlin) for support during the AUC measurements, and Melissa Gräwert and Manfred Roessle from the EMBL-SAXS beamline P12 for assistance with data collection.

Competing interests

The authors declare no competing or financial interests.

Author contributions

Y.S., E.R., C.S. and K.H-S. performed biochemical experiments. Y.S., K.Y. and S.S. performed cell biology experiments. Y.S. and Y.I. grew the crystals and determined the crystal structures. Y.S. and S.H-N. designed the expression constructs. Y.S., E.R., C.S., O.D. and S.S. wrote the paper.

Funding

This work was supported by grants from the Funding Program for Next Generation World-Leading Researchers (NEXT program); Japan Society for the Promotion of Science (JSPS) KAKENHI [grant number 26291037, 15H01641]; Astellas

Foundation for Research on Metabolic Disorders to S.S.; European Research Council (ERC) consolidator [grant number ERC-2013-CoG-616024 to O.D.]; and a grant of the German Research Foundation [grant number SFB958/A12].

Supplementary material

Supplementary material available online at
http://jcs.biologists.org/lookup/suppl/doi:10.1242/jcs.167775/-/DC1

References

Anggono, V., Koç-Schmitz, Y., Widagdo, J., Kormann, J., Quan, A., Chen, C.-M., Robinson, P. J., Choi, S.-Y., Linden, D. J., Plomann, M. et al. (2013). PICK1 interacts with PACSIN to regulate AMPA receptor internalization and cerebellar long-term depression. *Proc. Natl. Acad. Sci. USA* **110**, 13976-13981.

Boucrot, E., Howes, M. T., Kirchhausen, T. and Parton, R. G. (2011). Redistribution of caveolae during mitosis. *J. Cell Sci.* **124**, 1965-1972.

Braun, A., Pinyol, R., Dahlhaus, R., Koch, D., Fonarev, P., Grant, B. D., Kessels, M. M. and Qualmann, B. (2005). EHD proteins associate with syndapin I and II and such interactions play a crucial role in endosomal recycling. *Mol. Biol. Cell* **16**, 3642-3658.

Chachisvilis, M., Zhang, Y.-L. and Frangos, J. A. (2006). G protein-coupled receptors sense fluid shear stress in endothelial cells. *Proc. Natl. Acad. Sci. USA* **103**, 15463-15468.

Chou, C.-Y., Shen, M.-R., Hsu, K.-S., Huang, H.-Y. and Lin, H.-C. (1998). Involvement of PKC-alpha in regulatory volume decrease responses and activation of volume-sensitive chloride channels in human cervical cancer HT-3 cells. *J. Physiol.* **512**, 435-448.

Daumke, O., Lundmark, R., Vallis, Y., Martens, S., Butler, P. J. G. and McMahon, H. T. (2007). Architectural and mechanistic insights into an EHD ATPase involved in membrane remodelling. *Nature* **449**, 923-927.

Daumke, O., Roux, A. and Haucke, V. (2014). BAR domain scaffolds in dynamin-mediated membrane fission. *Cell* **156**, 882-892.

Davenport, K. R., Sohaskey, M., Kamada, Y., Levin, D. E. and Gustin, M. C. (1995). A second osmosensing signal transduction pathway in yeast. Hypotonic shock activates the PKC1 protein kinase-regulated cell integrity pathway. *J. Biol. Chem.* **270**, 30157-30161.

Del Pozo, M. A. and Schwartz, M. A. (2007). Rac, membrane heterogeneity, caveolin and regulation of growth by integrins. *Trends Cell Biol.* **17**, 246-250.

Ditchfield, C., Johnson, V. L., Tighe, A., Ellston, R., Haworth, C., Johnson, T., Mortlock, A., Keen, N. and Taylor, S. S. (2003). Aurora B couples chromosome alignment with anaphase by targeting BubR1, Mad2, and Cenp-E to kinetochores. *J. Cell Biol.* **161**, 267-280.

Echarri, A., Muriel, O., Pavon, D. M., Azegrouz, H., Escolar, F., Terron, M. C., Sanchez-Cabo, F., Martinez, F., Montoya, M. C., Llorca, O. et al. (2012). Caveolar domain organization and trafficking is regulated by Abl kinases and mDia1. *J. Cell Sci.* **125**, 3097-3113.

Franke, D. and Svergun, D. I. (2009). DAMMIF, a program for rapid ab-initio shape determination in small-angle scattering. *J. Appl. Crystallogr.* **42**, 342-346.

Folch, J., Lees, M. and Sloane-Stanley, G. (1957). A simple method for the isolation and purification of total lipids from animal tissues. *J. Biol. Chem.* **226**, 497-509.

Frost, A., Perera, R., Roux, A., Spasov, K., Destaing, O., Egelman, E. H., De Camilli, P. and Unger, V. M. (2008). Structural basis of membrane invagination by F-BAR domains. *Cell* **132**, 807-817.

Frost, A., Unger, V. M. and De Camilli, P. (2009). The BAR domain superfamily: membrane-molding macromolecules. *Cell* **137**, 191-196.

Fujita, A., Cheng, J., Tauchi-Sato, K., Takenawa, T. and Fujimoto, T. (2009). A distinct pool of phosphatidylinositol 4,5-bisphosphate in caveolae revealed by a nanoscale labeling technique. *Proc. Natl. Acad. Sci. USA* **106**, 9256-9261.

Gustincich, S., Vatta, P., Goruppi, S., Wolf, M., Saccone, S., Della Valle, G., Baggiolini, M. and Schneider, C. (1999). The human serum deprivation response gene (SDPR) maps to 2q32–q33 and codes for a phosphatidylserine-binding protein. *Genomics* **57**, 120-129.

Hansen, C. G., Howard, G. and Nichols, B. J. (2011). Pacsin 2 is recruited to caveolae and functions in caveolar biogenesis. *J. Cell Sci.* **124**, 2777-2785.

Hansen, C. G., Shvets, E., Howard, G., Riento, K. and Nichols, B. J. (2013). Deletion of cavin genes reveals tissue-specific mechanisms for morphogenesis of endothelial caveolae. *Nat. Commun.* **4**, 1831.

Hermoso, M., Olivero, P., Torres, R., Riveros, A., Quest, A. F. G. and Stutzin, A. (2004). Cell volume regulation in response to hypotonicity is impaired in HeLa cells expressing a protein kinase Calpha mutant lacking kinase activity. *J. Biol. Chem.* **279**, 17681-17689.

Hill, M. M., Bastiani, M., Luetterforst, R., Kirkham, M., Kirkham, A., Nixon, S. J., Walser, P., Abankwa, D., Oorschot, V. M. J., Martin, S. et al. (2008). PTRF-Cavin, a conserved cytoplasmic protein required for caveola formation and function. *Cell* **132**, 113-124.

Hill, M. M., Daud, N. H., Aung, C. S., Loo, D., Martin, S., Murphy, S., Black, D. M., Barry, R., Simpson, F., Liu, L. et al. (2012). Co-regulation of cell polarization and migration by caveolar proteins PTRF/cavin-1 and caveolin-1. *PLoS ONE* **7**, e43041.

Itoh, T. and De Camilli, P. (2006). BAR, F-BAR (EFC) and ENTH/ANTH domains in the regulation of membrane–cytosol interfaces and membrane curvature. *Biochim. Biophys. Acta* **1761**, 897-912.

Izumi, Y., Hirai, S.-i., Tamai, Y., Fujise-Matsuoka, A., Nishimura, Y. and Ohno, S. (1997). A protein kinase C delta-binding protein SRBC whose expression is induced by serum starvation. *J. Biol. Chem.* **272**, 7381-7389.

Jaqaman, K., Loerke, D., Mettlen, M., Kuwata, H., Grinstein, S., Schmid, S. L. and Danuser, G. (2008). Robust single-particle tracking in live-cell time-lapse sequences. *Nat. Methods* **5**, 695-702.

Kessels, M. M. and Qualmann, B. (2002). Syndapins integrate N-WASP in receptor-mediated endocytosis. *EMBO J.* **21**, 6083-6094.

Kessels, M. M. and Qualmann, B. (2004). The syndapin protein family: linking membrane trafficking with the cytoskeleton. *J. Cell Sci.* **117**, 3077-3086.

Koch, D., Westermann, M., Kessels, M. M. and Qualmann, B. (2012). Ultrastructural freeze-fracture immunolabeling identifies plasma membrane-localized syndapin II as a crucial factor in shaping caveolae. *Histochem. Cell Biol.* **138**, 215-230.

Konarev, P. V., Volkov, V. V., Sokolova, A. V., Koch, M. H. J. and Svergun, D. I. (2003). PRIMUS : a Windows PC-based system for small-angle scattering data analysis. *J. Appl. Crystallogr.* **36**, 1277-1282.

Konishi, H., Tanaka, M., Takemura, Y., Matsuzaki, H., Ono, Y., Kikkawa, U. and Nishizuka, Y. (1997). Activation of protein kinase C by tyrosine phosphorylation in response to H2O2. *Proc. Natl. Acad. Sci. USA* **94**, 11233-11237.

Kovtun, O., Tillu, V. A., Jung, W. R., Leneva, N., Ariotti, N., Chaudhary, N., Mandyam, R. A., Ferguson, C., Morgan, G. P., Johnston, W. A. et al. (2014). Structural insights into the organization of the cavin membrane coat complex. *Dev. Cell* **31**, 405-419.

Liu, X., Zhang, M. I. N., Peterson, L. B. and O'Neil, R. G. (2003). Osmomechanical stress selectively regulates translocation of protein kinase C isoforms. *FEBS Lett.* **538**, 101-106.

Ludwig, A., Howard, G., Mendoza-Topaz, C., Deerinck, T., Mackey, M., Sandin, S., Ellisman, M. H. and Nichols, B. J. (2013). Molecular composition and ultrastructure of the caveolar coat complex. *PLoS Biol.* **11**, e1001640.

Maciejewski, P. M., Peterson, F. C., Anderson, P. J. and Brooks, C. L. (1995). Mutation of serine 90 to glutamic acid mimics phosphorylation of bovine prolactin. *J. Biol. Chem.* **270**, 27661-27665.

Michelsen, P., Jergil, B. and Odham, G. (1995). Quantification of polyphosphoinositides using selected ion monitoring electrospray mass spectrometry. *Rapid Commun. Mass Spectrom.* **9**, 1109-1114.

Mineo, C., Ying, Y.-S., Chapline, C., Jaken, S. and Anderson, R. G. W. (1998). Targeting of protein kinase C alpha to caveolae. *J. Cell Biol.* **141**, 601-610.

Modregger, J., Ritter, B., Witter, B., Paulsson, M. and Plomann, M. (2000). All three PACSIN isoforms bind to endocytic proteins and inhibit endocytosis. *J. Cell Sci.* **113**, 4511-4521.

Mohan, J., Moren, B., Larsson, E., Holst, M. R. and Lundmark, R. (2015). Cavin3 interacts with cavin1 and caveolin1 to increase surface dynamics of caveolae. *J. Cell Sci.* **128**, 979-991.

Moren, B., Shah, C., Howes, M. T., Schieber, N. L., McMahon, H. T., Parton, R. G., Daumke, O. and Lundmark, R. (2012). EHD2 regulates caveolar dynamics via ATP-driven targeting and oligomerization. *Mol. Biol. Cell* **23**, 1316-1329.

Obi, S., Yamamoto, K., Shimizu, N., Kumagaya, S., Masumura, T., Sokabe, T., Asahara, T. and Ando, J. (2009). Fluid shear stress induces arterial differentiation of endothelial progenitor cells. *J. Appl. Physiol. (1985)* **106**, 203-211.

Ohno, S., Akita, Y., Konno, Y., Imajoh, S. and Suzuki, K. (1988). A novel phorbol ester receptor/protein kinase, nPKC, distantly related to the protein kinase C family. *Cell* **53**, 731-741.

Oka, N., Yamamoto, M., Schwencke, C., Kawabe, J.-i., Ebina, T., Ohno, S., Couet, J., Lisanti, M. P. and Ishikawa, Y. (1997). Caveolin interaction with protein kinase C: isoenzyme-dependent regulation of kinase activity by the caveolin scaffolding domain peptide. *J. Biol. Chem.* **272**, 33416-33421.

Ono, Y., Fujii, T., Ogita, K., Kikkawa, U., Igarashi, K. and Nishizuka, Y. (1988). The structure, expression, and properties of additional members of the protein kinase C family. *J. Biol. Chem.* **263**, 6927-6932.

Pelkmans, L. and Zerial, M. (2005). Kinase-regulated quantal assemblies and kiss-and-run recycling of caveolae. *Nature* **436**, 128-133.

Pelkmans, L., Bürli, T., Zerial, M. and Helenius, A. (2004). Caveolin-stabilized membrane domains as multifunctional transport and sorting devices in endocytic membrane traffic. *Cell* **118**, 767-780.

Peter, B. J., Kent, H. M., Mills, I. G., Vallis, Y., Butler, P. J. G., Evans, P. R. and McMahon, H. T. (2004). BAR domains as sensors of membrane curvature: the amphiphysin BAR structure. *Science* **303**, 495-499.

Petoukhov, M. V. and Svergun, D. I. (2005). Global Rigid Body Modeling of Macromolecular Complexes against Small-Angle Scattering Data. *Biophys. J.* **89**, 1237-1250.

Plomann, M., Wittmann, J. G. and Rudolph, M. G. (2010). A hinge in the distal end of the PACSIN 2 F-BAR domain may contribute to membrane-curvature sensing. *J. Mol. Biol.* **400**, 129-136.

Powell, K. A., Valova, V. A., Malladi, C. S., Jensen, O. N., Larsen, M. R. and Robinson, P. J. (2000). Phosphorylation of dynamin I on Ser-795 by protein

kinase C blocks its association with phospholipids. *J. Biol. Chem.* **275**, 11610-11617.

Qualmann, B., Roos, J., DiGregorio, P. J. and Kelly, R. B. (1999). Syndapin I, a synaptic dynamin-binding protein that associates with the neural Wiskott-Aldrich syndrome protein. *Mol. Biol. Cell* **10**, 501-513.

Quan, A., Xue, J., Wielens, J., Smillie, K. J., Anggono, V., Parker, M. W., Cousin, M. A., Graham, M. E. and Robinson, P. J. (2012). Phosphorylation of syndapin I F-BAR domain at two helix-capping motifs regulates membrane tubulation. *Proc. Natl. Acad. Sci. USA* **109**, 3760-3765.

Ramesh, P., Baroji, Y. F., Reihani, S. N. S., Stamou, D., Oddershede, L. B. and Bendix, P. M. (2013). FBAR syndapin 1 recognizes and stabilizes highly curved tubular membranes in a concentration dependent manner. *Sci. Rep.* **3**, 1565.

Rao, Y., Ma, Q., Vahedi-Faridi, A., Sundborger, A., Pechstein, A., Puchkov, D., Luo, L., Shupliakov, O., Saenger, W. and Haucke, V. (2010). Molecular basis for SH3 domain regulation of F-BAR-mediated membrane deformation. *Proc. Natl. Acad. Sci. USA* **107**, 8213-8218.

Robinson, P. J., Sontag, J.-M., Liu, J.-P., Fykse, E. M., Slaughter, C., McMahon, H. and Südhof, T. C. (1993). Dynamin GTPase regulated by protein kinase C phosphorylation in nerve terminals. *Nature* **365**, 163-166.

Safari, F. and Suetsugu, S. (2012). The BAR domain superfamily proteins from subcellular structures to human diseases. *Membranes* **2**, 91-117.

Schuck, P. (2003). On the analysis of protein self-association by sedimentation velocity analytical ultracentrifugation. *Anal. Biochem.* **320**, 104-124.

Senju, Y., Itoh, Y., Takano, K., Hamada, S. and Suetsugu, S. (2011). Essential role of PACSIN2/syndapin-II in caveolae membrane sculpting. *J. Cell Sci.* **124**, 2032-2040.

Sharma, D. K., Brown, J. C., Choudhury, A., Peterson, T. E., Holicky, E., Marks, D. L., Simari, R., Parton, R. G. and Pagano, R. E. (2004). Selective stimulation of caveolar endocytosis by glycosphingolipids and cholesterol. *Mol. Biol. Cell* **15**, 3114-3122.

Shimada, A., Niwa, H., Tsujita, K., Suetsugu, S., Nitta, K., Hanawa-Suetsugu, K., Akasaka, R., Nishino, Y., Toyama, M., Chen, L. et al. (2007). Curved EFC/F-BAR-domain dimers are joined end to end into a filament for membrane invagination in endocytosis. *Cell* **129**, 761-772.

Shimada, A., Takano, K., Shirouzu, M., Hanawa-Suetsugu, K., Terada, T., Toyooka, K., Umehara, T., Yamamoto, M., Yokoyama, S. and Suetsugu, S. (2010). Mapping of the basic amino-acid residues responsible for tubulation and cellular protrusion by the EFC/F-BAR domain of pacsin2/Syndapin II. *FEBS Lett.* **584**, 1111-1118.

Sinha, B., Köster, D., Ruez, R., Gonnord, P., Bastiani, M., Abankwa, D., Stan, R. V., Butler-Browne, G., Vedie, B., Johannes, L. et al. (2011). Cells respond to mechanical stress by rapid disassembly of caveolae. *Cell* **144**, 402-413.

Smart, E. J., Foster, D. C., Ying, Y. S., Kamen, B. A. and Anderson, R. G. (1994). Protein kinase C activators inhibit receptor-mediated potocytosis by preventing internalization of caveolae. *J. Cell Biol.* **124**, 307-313.

Smart, E. J., Ying, Y. S. and Anderson, R. G. (1995). Hormonal regulation of caveolae internalization. *J. Cell Biol.* **131**, 929-938.

Stoeber, M., Stoeck, I. K., Hänni, C., Bleck, C. K. E., Balistreri, G. and Helenius, A. (2012). Oligomers of the ATPase EHD2 confine caveolae to the plasma membrane through association with actin. *EMBO J.* **31**, 2350-2364.

Suetsugu, S. and Gautreau, A. (2012). Synergistic BAR–NPF interactions in actin-driven membrane remodeling. *Trends Cell Biol.* **22**, 141-150.

Suetsugu, S., Toyooka, K. and Senju, Y. (2010). Subcellular membrane curvature mediated by the BAR domain superfamily proteins. *Semin. Cell Dev. Biol.* **21**, 340-349.

Suetsugu, S., Kurisu, S. and Takenawa, T. (2014). Dynamic shaping of cellular membranes by phospholipids and membrane-deforming proteins. *Physiol. Rev.* **94**, 1219-1248.

Svergun, D., Barberato, C. and Koch, M. H. J. (1995). CRYSOL – a Program to Evaluate X-ray Solution Scattering of Biological Macromolecules from Atomic Coordinates. *J. Appl. Crystallogr.* **28**, 768-773.

Takeda, T., Robinson, I. M., Savoian, M. M., Griffiths, J. R., Whetton, A. D., McMahon, H. T. and Glover, D. M. (2013). Drosophila F-BAR protein Syndapin contributes to coupling the plasma membrane and contractile ring in cytokinesis. *Open Biol.* **3**, 130081.

Wang, Q., Navarro, M. V. A. S., Peng, G., Molinelli, E., Goh, S. L., Judson, B. L., Rajashankar, K. R. and Sondermann, H. (2009). Molecular mechanism of membrane constriction and tubulation mediated by the F-BAR protein Pacsin/Syndapin. *Proc. Natl. Acad. Sci. USA* **106**, 12700-12705.

Wriggers, W. (2010). Using Situs for the integration of multi-resolution structures. *Biophys. Rev.* **2**, 21-27.

Xue, Y., Liu, Z., Cao, J., Ma, Q., Gao, X., Wang, Q., Jin, C., Zhou, Y., Wen, L. and Ren, J. (2011). GPS 2.1: enhanced prediction of kinase-specific phosphorylation sites with an algorithm of motif length selection. *Protein Eng. Des. Sel.* **24**, 255-260.

Yamamoto, K., Shimizu, N., Obi, S., Kumagaya, S., Taketani, Y., Kamiya, A. and Ando, J. (2007). Involvement of cell surface ATP synthase in flow-induced ATP release by vascular endothelial cells. *Am. J. Physiol. Heart Circ. Physiol.* **293**, H1646-H1653.

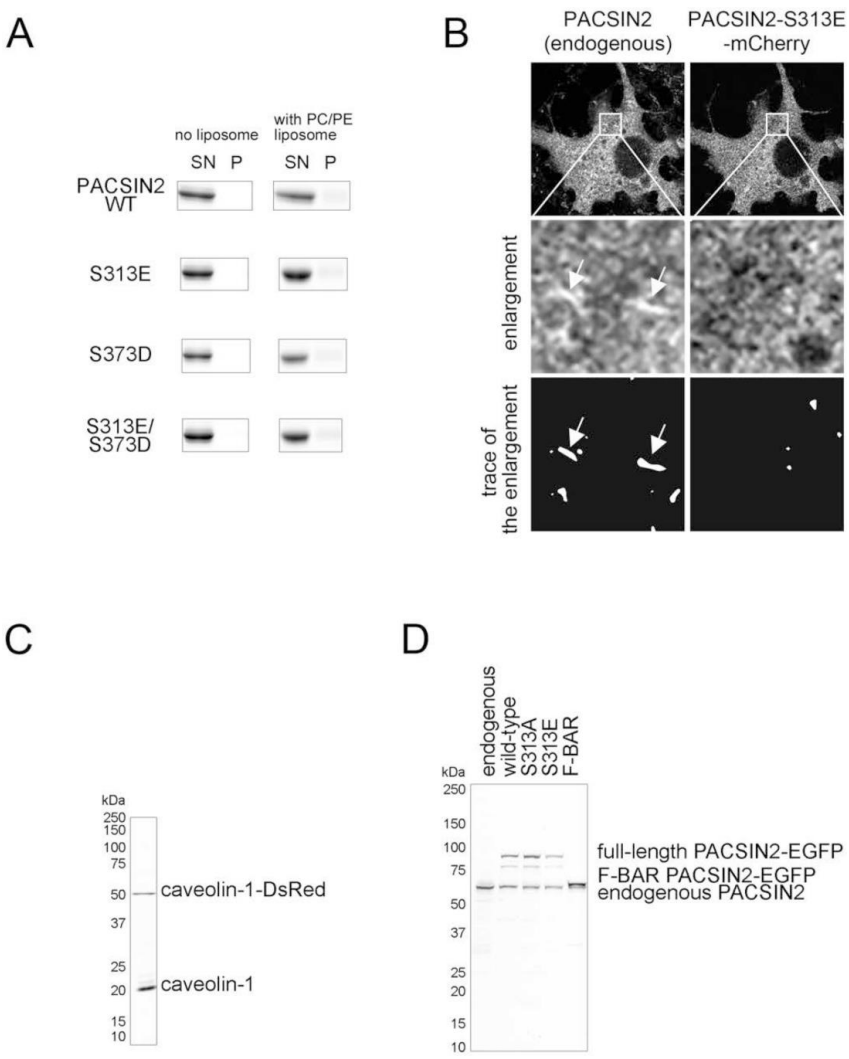

Figure S1. Characterization of the PACSIN2 phosphorylation.

(**A**) PACSIN2 binding to liposomes made of PC and PE. PACSIN2 binding to liposomes made of PC and PE was analyzed as in Figure 3A. (**B**) Endogenous PACSIN2 tubules. Non-transfected Hela cells (left) or HeLa cells expressing PACSIN2 S313E-mCherry were stained with an anti-PACSIN2 antibody to detect endogenous PACSIN2. The area marked with rectangles in the upper images was enlarged in the middle images. The tubular structures of the endogenous PACSIN2 are shown with arrows. For better visualization, higher signals of the middle images are shown on the bottom. (**C**) Exogenous caveolin-1 expression in Hela cells. Representative western blot with the anti-caveolin-1 antibody in Hela cells stably expressing caveolin-1-DsRedm. Based on this blot, we estimate that caveolin-1-DsRedm expressed at a level of approximately 25% compared to endogenous caveolin-1. (**D**) Exogenous PACSIN2 expression in Hela cells. Representative western blot with the anti-PACSIN2 antibody detecting PACSIN2-GFP and endogenous PACSIN2. Since the transfection efficiency was approximately 50-70%, the amount of exogenously expressed PACSIN2 was approximately 2 times higher than that of the endogenous protein.

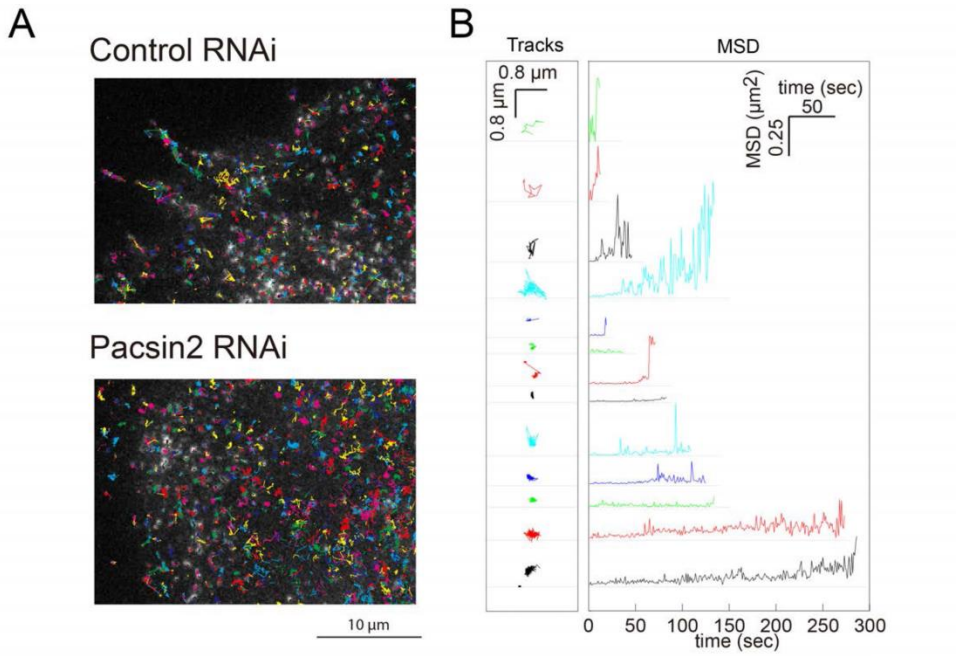

Figure S2. Representative results of caveolin-1 spot tracking.

(**A**) Caveolin-1 spots on control or PACSIN2 RNAi-treated cells were tracked, and the tracks formed during 25 seconds are shown. Each track is differentially colored, and colors are not related to the tracked durations.

(**B**) Plots of MSDs and tracks from randomly chosen caveolae over time from a cell treated with control RNAi.

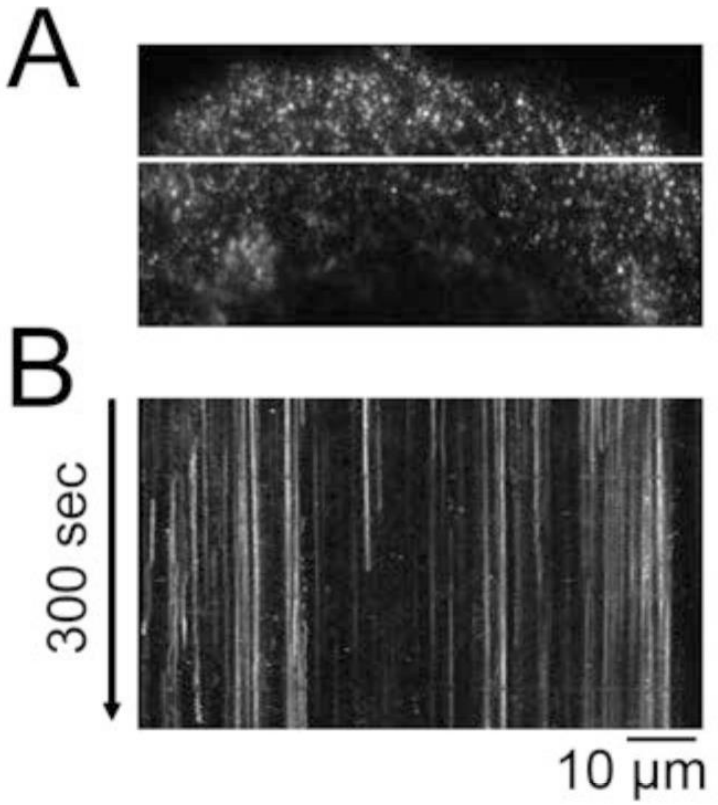

Figure S3. PMA treatment of caveolin-1-GFP-expressing Flp-in T-REx Hela cells. (**A**) Caveolin-1-GFP fluorescence was monitored for 300 sec after cells were treated with PMA for 1 min, as in Figure 5. (**B**) The kymograph over 300 seconds was generated from the indicated line. Dotted vertical lines in kymographs indicate shorter tracking durations of caveolae.

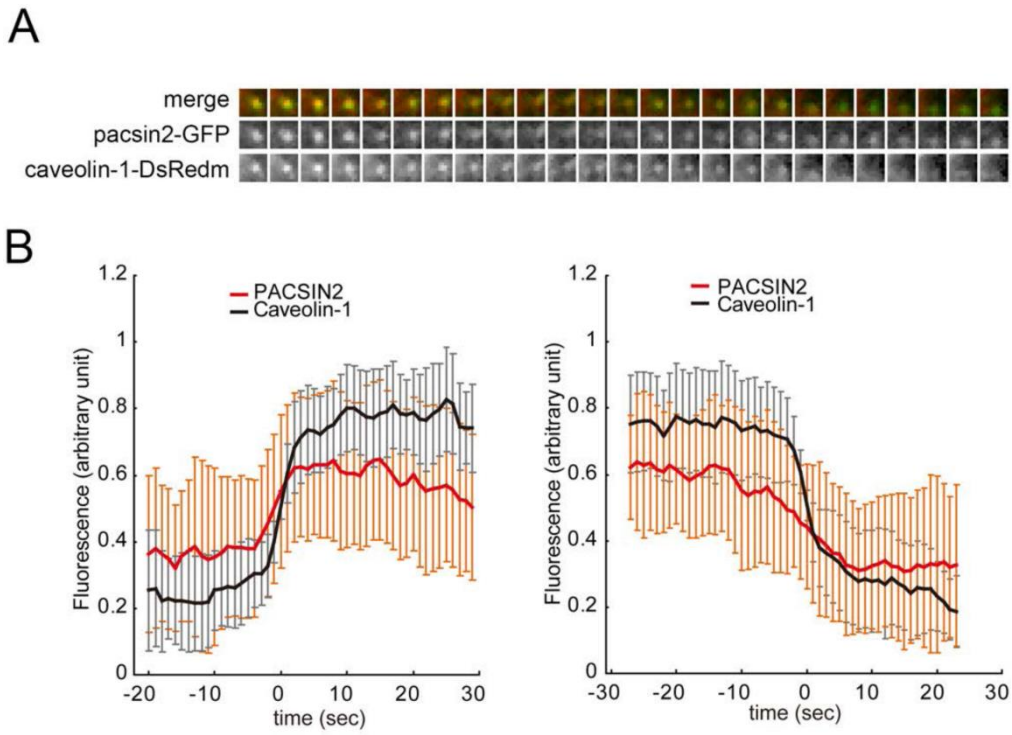

Figure S4. Time courses of PACSIN2 and caveolin-1 localizations.

(**A**) TIRF images of HeLa cells transfected with PACSIN2-GFP (green) and stably transfected with caveolin-1-DsRedm (red). Representative sequential images of disappearance of caveolin-1 are shown.

(**B**) Quantification of the fluorescence intensity of PACSIN2 and caveolin-1 before and after the appearance (left, 0 time point) and disappearance (right, 0 time point) of a caveolin-1 signal at the plasma membrane. Mean ± S.D. (n= 51, 71).

MOVIE 1. HeLa cells stably expressing caveolin-1-DsRedm after treatment with control or PACSIN2 siRNA, visualized by TIRF microscopy.

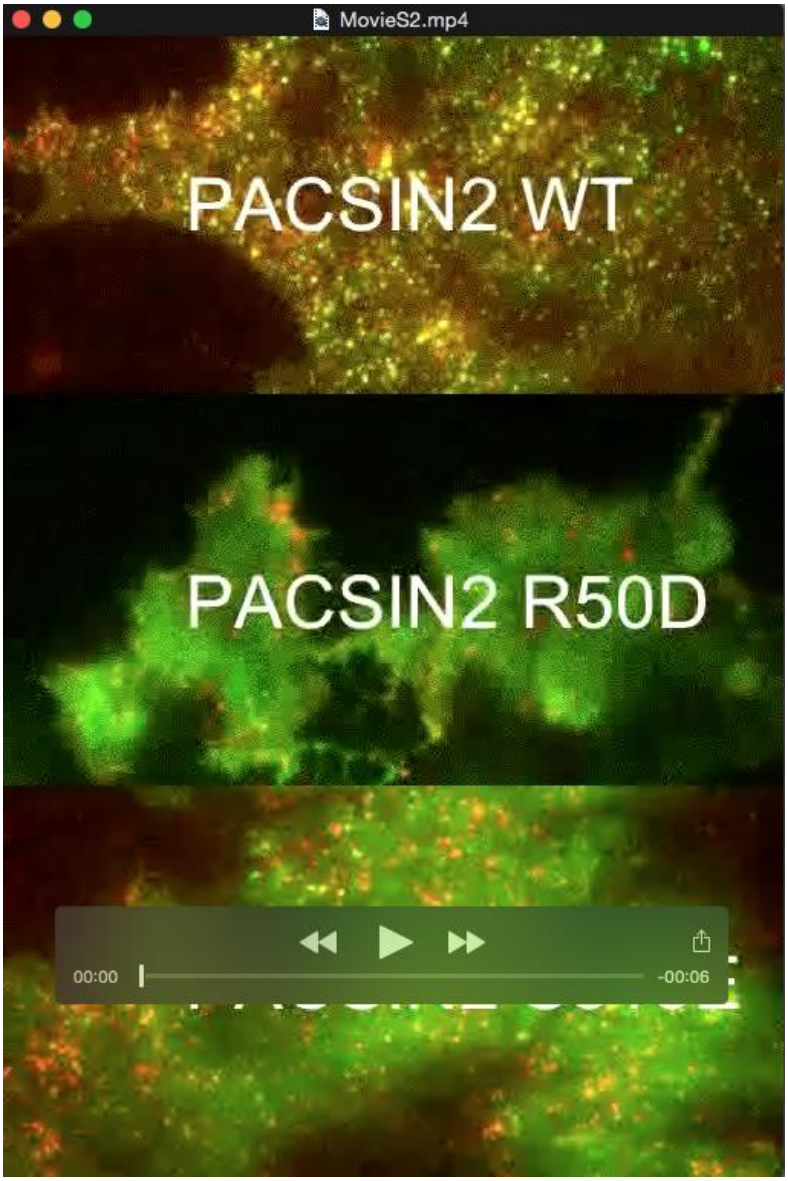

MOVIE 2. HeLa cells stably expressing caveolin-1-DsRedm (red) and WT, R50D, or S313E PACSIN2-GFP (green), visualized by TIRF microscopy.

MOVIE 3. HeLa cells stably expressing caveolin-1-DsRedm after 1 min of treatment with PMA, visualized by TIRF microscopy.

MOVIE 4. HeLa cells stably expressing caveolin-1-DsRedm after 1 min of treatment with hypotonic medium, visualized by TIRF microscopy.

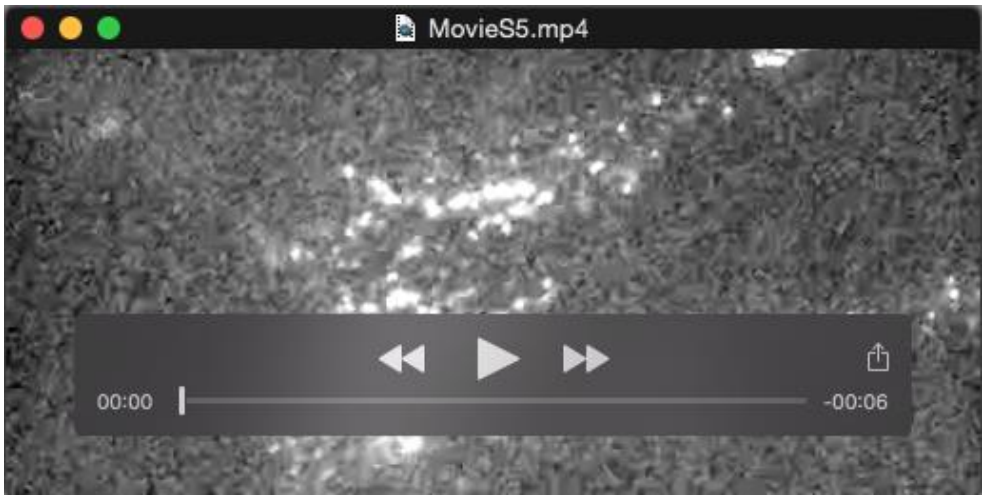

MOVIE 5. HeLa cells stably expressing caveolin-1-DsRedm after treatment with BIM and hypotonic conditions, visualized by TIRF microscopy.

MOVIE 6. HeLa cells expressing WT PACSIN2-GFP (green) and stably expressing caveolin-1-DsRedm (red) after hypotonic treatment, visualized by TIRF microscopy.

MOVIE 7. Flp-In T-REx HeLa cells expressing caveolin-1-GFP after 1 min of treatment with PMA, visualized by TIRF microscopy.

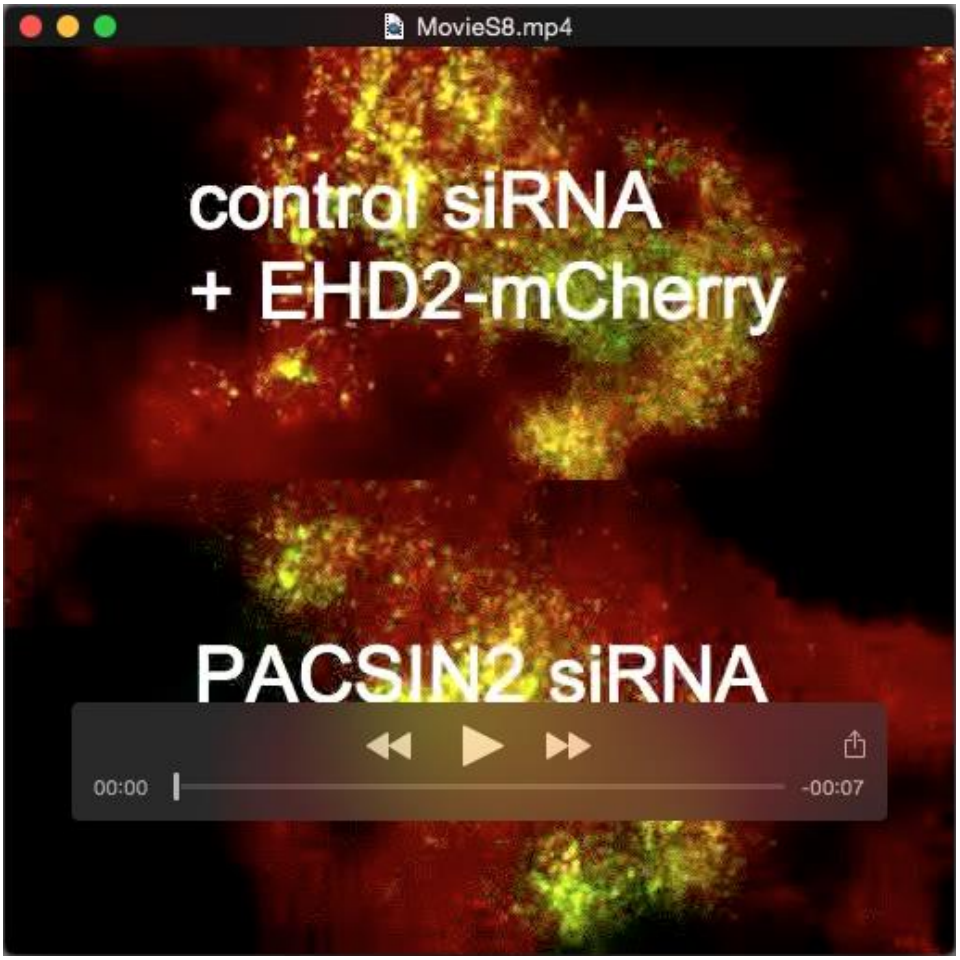

MOVIE 8. HeLa cells stably expressing caveolin-1-GFP (green) and expressing EHD2-mCherry (red) and after treatment with control or PACSIN2 siRNA, visualized by TIRF microscopy.